Received: 1 December 2022 | Revised: 18 January 2023 | Accepted: 19 January 2023

DOI: 10.1002/glia.24352

GLIA

WILEY

RESEARCH ARTICLE

Dysfunction of NG2 glial cells affects neuronal plasticity and behavior

Aline Timmermann[1] | Dario Tascio[1] | Ronald Jabs[1] | Anne Boehlen[1] | Catia Domingos[1] | Magdalena Skubal[1] | Wenhui Huang[2] | Frank Kirchhoff[2] | Christian Henneberger[1,3,4] | Andras Bilkei-Gorzo[5] | Gerald Seifert[1] | Christian Steinhäuser[1]

[1]Institute of Cellular Neurosciences, Medical Faculty, University of Bonn, Bonn, Germany

[2]Molecular Physiology, Center for Integrative Physiology and Molecular Medicine (CIPMM), University of Saarland, Homburg, Germany

[3]German Center for Neurodegenerative Diseases (DZNE), Bonn, Germany

[4]Institute of Neurology, University College London, London, UK

[5]Institute of Molecular Psychiatry, Medical Faculty, University of Bonn, Bonn, Germany

Correspondence
Christian Steinhäuser, Institute of Cellular Neurosciences, Medical Faculty, University of Bonn, Venusberg-Campus 1, 53127 Bonn, Germany.
Email: cste@uni-bonn.de

Funding information
Deutsche Forschungsgemeinschaft, Grant/Award Numbers: HE 6949/3, SPP1757,HE6949/1, SPP1757,SE 774/6, SPP1757,STE 552/5

Abstract

NG2 glia represents a distinct type of macroglial cells in the CNS and is unique among glia because they receive synaptic input from neurons. They are abundantly present in white and gray matter. While the majority of white matter NG2 glia differentiates into oligodendrocytes, the physiological impact of gray matter NG2 glia and their synaptic input are still ill defined. Here, we asked whether dysfunctional NG2 glia affect neuronal signaling and behavior. We generated mice with inducible deletion of the K^+ channel Kir4.1 in NG2 glia and performed comparative electrophysiological, immunohistochemical, molecular and behavioral analyses. Kir4.1 was deleted at postnatal day 23–26 (recombination efficiency about 75%) and mice were investigated 3–8 weeks later. Notably, these mice with dysfunctional NG2 glia demonstrated improved spatial memory as revealed by testing new object location recognition while working and social memory remained unaffected. Focussing on the hippocampus, we found that loss of Kir4.1 potentiated synaptic depolarizations of NG2 glia and stimulated the expression of myelin basic protein while proliferation and differentiation of hippocampal NG2 glia remained largely unaffected. Mice with targeted deletion of the K^+ channel in NG2 glia showed impaired long-term potentiation at CA3-CA1 synapses, which could be fully rescued by extracellular application of a TrkB receptor agonist. Our data demonstrate that proper NG2 glia function is important for normal brain function and behavior.

KEYWORDS
Kir4.1, myelination, neuronal plasticity, neuron–glia signaling, NG2 glia

1 | INTRODUCTION

NG2 glial cells, which have also been termed complex cells, GluR cells, synantocytes, oligodendrocyte precursor cells, or polydendrocytes (reviewed by Bergles et al., 2010), represent a distinct type of macroglial cells in the CNS (Nishiyama et al., 2009; Peters, 2004). They are unique among glia because they receive direct synaptic input from glutamatergic and GABAergic neurons (Bergles et al., 2000; Jabs et al., 2005; Lin & Bergles, 2004). NG2 glia are abundantly present in white and gray matter, make up about 5%–10% of total glial cell

numbers and display variability with regard to their functional properties and antigen profiles (Degen et al., 2012; Marisca et al., 2020; Seifert & Steinhäuser, 2018; Trotter et al., 2010). They have a high proliferative potential and, in gray matter, many cells keep their NG2 glia phenotype throughout adulthood (Dimou et al., 2008; Kang et al., 2010; Moshrefi-Ravasdjani et al., 2017). Despite intense research, the physiological impact of gray matter NG2 glia and their synaptic innervation are yet largely unknown. This deficit is mainly due to the fact that NG2 glia express a similar set of ion channels and receptors as neurons, although often at a much lower density, which makes selective manipulation of the glial cells difficult. To circumvent this problem, cell-type specific genetic deletion strategies have been developed. Thus, it has been demonstrated that ablation of NG2 cells entails depressive-like behavior (Birey et al., 2015) and impairs microglial function (Liu & Aguzzi, 2020), and deletion of AMPA receptors in NG2 glia affected white matter myelination (Kougioumtzidou et al., 2017).

The neurophysiological fingerprint of NG2 glia is mainly determined by the inward rectifier K^+ channel Kir4.1 that is developmentally upregulated and dominates the membrane conductance in the physiologically relevant voltage range (Djukic et al., 2007; Schröder et al., 2002; Tang et al., 2009); reviewed by (Seifert & Steinhäuser, 2018), which allows them to sense $[K^+]_o$ (Maldonado et al., 2013). Thus, one promising approach to learn about NG2 glia function is to delete this important signaling molecule, to disturb normal NG2 glia function and test whether this entails altered neuronal function. Recently, Larson et al. generated mice with tamoxifen-induced deletion of Kir4.1 in PDGFRα^+ NG2 glia. As expected, Kir4.1-lacking NG2 glia were significantly depolarized, but their survival, proliferation and differentiation were not affected (Larson et al., 2018). A similar approach was used by Song et al. to show that deletion of Kir4.1 from NG2 glia contributes to myelin loss in a transient ischemic mouse model (Song et al., 2018).

These findings imply that dysfunctional NG2 glia can affect neuronal signaling and mouse behavior. We tested this hypothesis by using NG2-CreERT2 knockin mice to inducibly delete Kir4.1 from NG2 glia. These mice demonstrated improved spatial memory as revealed by testing object location recognition. Focussing on the hippocampus, we demonstrate that loss of the K^+ conductance significantly potentiated synaptic depolarizations of the glial cells, which was accompanied by an upregulation of myelin basic protein (MBP) on the transcript and protein levels. Moreover, mice with targeted deletion of Kir4.1 in NG2 glia showed impaired LTP at CA3-CA1 synapses, which could be rescued by a TrkB receptor agonist. Thus, our data demonstrate that proper NG2 glia function is required for normal brain function and behavior.

2 | MATERIALS AND METHODS

Experiments were performed with NG2ki-EYFP (Karram et al., 2008) and NG2-CreERT2 × Kir4.1$^{fl/fl}$; Rosa26-STOP$^{fl/fl}$-EYFP mice (hereinafter referred to as Kir4.1 ko mice). The latter were obtained by cross breeding mice carrying the floxed Kir4.1 gene (Kir4.1 fl/fl) with knockin mice expressing the Cre DNA recombinase variant CreERT2 in the NG2 (*cspg4*) locus (NG2-CreERT2 × Rosa26-EYFP) as previously described (Huang et al., 2014). NG2-CreERT2 × Rosa26-EYFP mice (without floxed Kir4.1) were used as controls. In both transgenic lines, Rosa26-floxed-stop-EYFP (Rosa26-EYFP) is used as a reporter to monitor Cre activity (Huang et al., 2014; Srinivas et al., 2001). Mice were kept under standard housing conditions (12/12 h light/dark cycle, food, and water ad libitum). All experiments were carried out in accordance with local, state and European regulations (veterinary licenses 84-02.04.2015.A411, 81-02.04.2017.A437).

2.1 | Tamoxifen administration

Mice of either sex (p23-26) were intraperitoneally injected with 1.5 mg tamoxifen (Sigma) dissolved in ethanol (AppliChem, Roth) and sunflower seed oil (Sigma) in a ratio of 1:10. Animals were injected once per day for three consecutive days (Huang et al., 2014). Electrophysiological and immunohistochemical analyses were performed 3–4 and 8 wpi, respectively. For the behavioral experiments the mice were introduced to the tasks in the third week after tamoxifen.

2.2 | Behavioral tests

Behavioral tests were performed as previously reported (Albayram et al., 2016; Bilkei-Gorzo et al., 2017). For the Y-maze test, the length of the arms of the Y-shaped labyrinth was 20 cm and the height of their walls was 15 cm. Animals were placed into the end of one of the arms and their location and activity was recorded and analyzed by the EthoVision tracking system (Noldus) for 10 min. The ration of spontaneous alternations was defined as entering a different arm in 3 consecutive arm entries. Percent value was calculated as SA/TA-2*100, where SA is the number of spontaneous alternations and TA is the total number of arm entries. The maze was thoroughly cleaned using detergent between the animals to avoid odor cues.

The novel object location recognition test was performed in a sound-isolated, dimly illuminated room in an open field-box (44 × 44 cm^2). The floor was covered with sawdust (1 cm deep, saturated with the odor of the animals during habituation). The habituation period consisted of a daily 5-min period of free exploration in the arena for 3 days. On day 4, the animals were allowed to explore three identical objects (LEGO pieces with different colors, roughly 2 × 2 cm^2) placed into the area in a fixed location for 6 min, and the time spent on the inspection of the individual objects was recorded (Noldus Ethovision, XT software). Thirty minutes later the animals were placed back into the box, where one object was placed into a new location. The animals were left to explore for an additional 3 min. The time spent with investigations was recorded, and the preference ratio for the moved object was calculated as follows: Preference $= T_a/(T_a + T_b + T_c)$*100, where T is the time spent with investigation, a – object which is moved in the second trial, b and

c objects remained in the original position. Novelty preference was calculated as (Pt2-Pt1)/Pt1*100, where *P* is the preference, t1 is trial 1 and t2 is trial 2.

The partner recognition test was performed in the same arenas and after the same habituation as described for the novel object location recognition test. In the first trial, the arenas contained a metal grid cage, with a mouse in one cage (same age and sex as the test animal, from different cage) and an object (similar size and form as the metal grid cage) in the opposing corner 6–7 cm from the walls. Location and activity of the test mouse were recorded (15 min) and analyzed (EthoVision tracking system, Noldus). In the next trial, the object was replaced with another grid cage containing a new partner and the activity of the test mouse was recorded again (5 min). The inter-trial interval was 1 h on day 4, whereas 2, 4 and 8 h on day 5, 6 and 7, respectively. Recognition of the previously seen partner was defined by a novelty preference, that is, a significantly higher period spent investigating the new partner in the second trial. Novelty preference was calculated as $(T_a - T_b)/T_b$*100, where T_a is the time spent with the novel, and T_b is the time spent with the previous partner.

2.3 | Slice preparation

Mice were anesthetized with 50% O_2/50% CO_2 or isoflurane before decapitation. Horizontal slices of 200–300 μm thickness were obtained with a vibratome (Leica VT1000S/1200 S; Leica Microsystems) in ice cold slicing solution containing (in mM): 87 NaCl, 2.5 KCl, 1.25 NaH_2PO_4, 7 $MgCl_2$, 0.5 $CaCl_2$, 25 $NaHCO_3$, 25 glucose, 61.3 sucrose. Sections were incubated for 15 min at 35°C in the same solution before being stored at room temperature in artificial cerebrospinal fluid (aCSF; in mM: 132 NaCl, 3 KCl, 2 $MgCl_2$, 2 $CaCl_2$, 10 glucose, 1.25 NaH_2PO_4, 20 $NaHCO_3$) until further use. For extracellular field potential recordings, the bath solution contained (in mM) 131 NaCl, 2.5 KCl, 1.3 $MgSO_4$, 1.25 NaH_2PO_4, 21 $NaHCO_3$, 2 $CaCl_2$, 10 glucose. Solutions were oxygenated with carbogen (5% CO_2/95% O_2). Slices were allowed to recover for at least 1 h before experiments.

2.4 | Patch-clamp recordings

Slices were transferred to a recording chamber on an upright microscope (Axioskop FS2, Zeiss, equipped with a CCD camera, VX45, Optronics, Infrared-DIC optics, Eclipse E600 FN, Nikon, and epifluorescence, Polychrome II, Till Photonics), and constantly perfused with oxygenated aCSF. NG2 glial cells located in the hippocampal CA1 stratum radiatum were identified by intrinsic EYFP expression after induction of Cre mediated recombination by tamoxifen. Borosilicate capillaries (Science Products) pulled by a horizontal puller (P-87; Sutter Instrument) had a resistance of 3–5 MΩ when filled with either of the following intracellular solutions (in mM): 125 K-gluconate, 20 KCl, 3 NaCl, 2 $MgCl_2$, 0.5 EGTA, 3 Na_2-ATP, 10 HEPES (for recording of miniature postsynaptic potentials (mPSPs) and miniature postsynaptic currents (mPSCs); liquid junction potential corrected) or 130 KCl, 2 $MgCl_2$, 0.5 $CaCl_2$, 3 Na_2-ATP, 5 BAPTA, 50 μM spermine, 10 HEPES (for evoked EPSC recordings). Cells were clamped to −80 mV, and series and input resistance were constantly monitored applying 10 mV voltage steps. Whole cell patch-clamp recordings were obtained using an EPC800 amplifier (HEKA Electronic) and digitized with an ITC 16 D/A converter (HEKA Electronic). Signals were filtered at 1 or 10 kHz, sampled at 6, 10 or 30 kHz and displayed by Tida software (HEKA Electronic). In the current-clamp mode, voltage signals were amplified with a DPA 2FS amplifier (npi electronic). Experiments were performed at 35°C if not stated otherwise.

Passive membrane properties were determined after establishing the whole-cell configuration. The average of 10 consecutive transients evoked by 50 ms lasting 10 mV voltage step was used to determine series resistance (Rs), membrane resistance (Rm) and membrane capacitance (Cm). As it is currently impossible to properly determine resistances above 3 GΩ due to technical reasons, data above this threshold was excluded from analysis. mPSPs and mPSCs were recorded (8 min periods) in aCSF containing TTX (0.5 μM; Abcam). Recordings were sampled at 6 kHz and filtered at 1 kHz. For mPSP recordings, NBQX (10 μM; Tocris) and/or Picrotoxin (150 μM; Abcam) were added via the perfusion system to separate GABAergic and glutamatergic inputs. mPSPs and mPSCs were detected using the template search of pClamp (Molecular devices) and evaluated by visual inspection. Cells with less than two events detected were rejected. For mPSCs, templates with fast and slow decay kinetics were used to separate AMPA- and $GABA_A$-receptor mediated currents. Only mPSCs with decay time constants below 15 ms were considered as AMPA receptor mediated. Cells were clamped close to the their respective resting membrane potentials, that is, control cells to −80 mV and Kir 4.1 ko cells to −60 mV. Consequently, mPSC amplitudes were extrapolated to −70 mV holding potential assuming a linear I/V curve between −80 and − 60 mV. Amplitudes, kinetics and frequencies of mPSPs and mPSCs were analyzed by a custom-written macro in IGOR Pro Software (WaveMetrics).

2.5 | Schaffer collateral stimulation

Schaffer collaterals were stimulated using a monopolar stimulation electrode consisting of a teflon-coated silver wire and a low-resistance glass pipette (<1 MΩ) filled with aCSF. The pipette was placed in the CA1 stratum radiatum and stimulus intensity was adjusted to stimulate single or few presynaptic fibers (minimal stimulation). Paired pulse stimulation was induced by biphasic voltage pulses of 150 μs duration and inter-stimulus intervals of 50 ms, applied via an AM-Systems isolation pulse stimulator (Model 2100, A-M Systems). Recombined NG2 glial cells were recorded with KCl-based intracellular solution. A response was considered a failure if the current amplitude was less than twice the baseline noise, verified by visual inspection. Recordings were analyzed by a custom-written macro in IGOR Pro Software (WaveMetrics).

2.6 | Field potential recordings

Experiments were performed in an interface chamber (IFC) (custom-made, AG Heinemann, Charité-Universitätsmedizin Berlin), and slices were continuously perfused with carbogenated aCSF (34.0 ± 0.5°C; flow rate, 2.5 ± 0.2 mL/min). For stimulation, a concentric bipolar electrode was used (CBARC75; FHC) and stimulus intensity was controlled by an isolated current stimulator (DS3, Digitimer Ltd.). Signals were pre-amplified, filtered (highpass 0.1 Hz, lowpass 20 kHz; EXT-02B, npi) and 50 Hz-interferences were removed (HumBug, Quest Scientific Instruments, Inc.). Signals were sampled at a frequency of 10 kHz (NI USB-6221, National Instruments). Hippocampal evoked field excitatory postsynaptic potentials (fEPSPs) were recorded in the CA1 stratum radiatum using patch pipettes (resistance 3–8 MΩ) filled with aCSF. Input–output curves were obtained with increasing stimulation intensities (range: 20–500 μA). Each stimulus intensity was delivered 3 times, mean values were calculated and the initial slope of the fEPSPs was evaluated. Baseline paired-pulse (inter-stimulus interval 50 ms) or single pulse (100 μs duration) recordings were obtained every 15 s for 10 min. LTP was induced by theta burst stimulations (TBS), applying 8 stimulus trains at 5 Hz (4 pulses at 100 Hz; 1 min inter-stimulus interval, 3 repetitions). After TBS, baseline stimulation was repeated for further 30 min (120 pulses). Stimulation intensity was adjusted to evoke half-maximal fEPSP amplitudes. Analysis was performed with Clampfit (V. 10.3; Molecular Devices, LLC). fEPSPs elicited by paired-pulse stimulation were normalized to the mean fEPSP slopes obtained during the first 10 min of the experiment (baseline). To evaluate LTP, responses recorded before (baseline, 10 min) and after TBS were normalized to the mean fEPSP slope during baseline recording and the ratio of fEPSP slopes was calculated (paired-pulse ratio = slope 2 / slope 1). Recordings with more than 10% fEPSP slope variability during baseline recording were excluded. Bath application of the TrkB receptor agonist 7,8-dihydroxyflavone (7,8-DHF; Sigma-Aldrich) started 50 min before TBS.

2.7 | FACsorting of NG2 glial cells

Mice of both sexes (NG2ki-EYFP at p60; Kir4.1 ko and NG2CreERT2xRosa26-EYFP (control) mice 3wpi) were sacrificed, their brains were dissected, and whole hippocampi were isolated under microscopic control (Stereo microscope, Zeiss, Germany). Cell suspensions were prepared by mincing and digesting the tissue in papain (37°C, 15 min). Then, DNAseI was added (incubation for another 10 min; Neural Dissociation Kit (P), Miltenyi, Germany). The tissue was dissociated by Pasteur pipettes, filtered through a 70 μm cell strainer and centrifuged (300*g*, 10 min) after addition of 10 mL HBSS (with Ca^{2+} and Mg^{2+}). The pellet was re-suspended in 1 mL HBSS (without Ca^{2+} and Mg^{2+}), filtered through a 40 μm cell strainer. NG2 cells were identified by their fluorescence (emission at 527 nm) and sorted by a FACSAriaIII flow cytometer (70 μm nozzle, BD Biosciences, Heidelberg, Germany) into tubes in HBSS (without Ca^{2+} and Mg^{2+}). After centrifugation at 2000*g* (10 min) the supernatant was discarded, the cells were re-suspended in 200 μL lysis/binding buffer (Invitrogen, Darmstadt, Germany), frozen in liquid nitrogen and stored at −80 °C.

2.8 | Semiquantitative real-time RT-PCR

Messenger RNA was isolated from isolated cells by cell lysis in the lysis/binding buffer and by using oligo(dT)25-linked Dynabeads (Invitrogen). The beads with adherent mRNA were suspended in DEPC-treated water (20 μL). For first strand synthesis, first strand buffer (Invitrogen), dithiothreitol (DTT, 10 mM), dNTPs (4 × 250 μM, Applied Biosystems), oligo-dT_{24}-primer (5 μM, Eurogentec), RNasin (80 U, Promega) and SuperscriptIII reverse transcriptase (400 U, Invitrogen) were added and the reaction mix was incubated for 1 h at 50 °C (final volume 40 μL). The reaction mixture for real-time PCR contained Takyon real-time PCR mastermix (Eurogentec) and Taqman primer/probe mix (Applied Biosystems, Darmstadt, Germany), and 1 μL of the RT-product was added (reaction volume 12.5 μL). PCRs for the respective target genes and β-actin as a housekeeping gene were run in parallel wells for each sample, respectively and triplicates for each sample were performed. Negative controls (water) were also performed in each run. Samples were incubated at 50°C (2 min), and after denaturation (95°C, 10 min), 50 cycles were performed (denaturation at 95 °C, 15 s; primer annealing and extension at 60°C, 60 s). Fluorescence intensity was readout during each annealing/extension step (CFX 384, Biorad, Munich, Germany). The target gene/β-actin gene expression ratio was determined by comparing C_T values of the target gene with those of the reference gene. The relative quantification of different genes was determined according to the following equation:

$$X_{\text{target}}/X_{\beta-\text{actin}} = E_{\beta-\text{actin}}{}^{\text{CT}\beta-\text{actin}}/E_{\text{target}}{}^{\text{CTtarget}}, \quad (1)$$

yielding the gene ratio with X being the input copy number, E the efficiency of amplification, and C_T the cycle number at threshold. By quantification of target gene expression against that of β-actin, C_T was determined for each gene at the same fluorescence emission, R_n. The amplification efficiency was determined by serial dilutions of mRNA and was 1.93 for Kir4.1, 1.94 for β-actin, 1.91 for MAG and 1.89 for MBP.

2.9 | Single-cell RT-PCR

Single-cell transcript analysis was performed as previously reported (Matthias et al., 2003). Briefly, after recording, the cytoplasm of individual cells was harvested under microscopic control (Axioskop FSII, Zeiss, equipped with a CCD camera VX45, Optronis, Kehl, Germany) and aspirated in reaction tubes filled with 3 μL DEPC-treated water. Reverse transcription (RT) was performed after addition of the first strand buffer (Invitrogen), dithiothreitol (DTT; 10 mM), dNTPs (4x 250 μM), random hexamer primers (50 μM; Roche), RNasin (20 U;

TABLE 1 Membrane properties of control, Kir4.1 wt and Kir4.1 ko cells.

	Control	Kir4.1 wt	Kir4.1 ko
RMP (mV)	−89	−85	−61
	(−90 to −86)	(−89 to −82)	(−69 to −53)
	[82]	[55]	[128]
Rm (MΩ)	50.75	81.22	546.10
	(32.69–81.75)	(56.56–115.17)	(348.94–1022.90)
	[82]	[55]	[118]
Cm (pF)	29.98	31.09	27.28
	(25.68–35.66)	(24.92–38.16)	(23.09–33.89)
	[82]	[55]	[128]
Conductance at − 130 mV (pA/mV)	17.42	12.81	1.40
	(13.78–22.62)	(9.77–17.46)	(0.93–2.05)
	[82]	[55]	[128]

Note: Data are given as median and interquartile range (quartile 25%–quartile 75%), number of cells in square brackets.
Abbreviations: RMP, resting membrane potential; Rm, membrane resistance; Cm, membrane capacitance.

Promega) and SuperscriptIII reverse transcriptase (100 U; Invitrogen) at 37°C for 1 h. A multiplex two-round single-cell PCR was performed with primers for Kir4.1 and PDGFRα (Table 1). The first PCR was performed after adding PCR buffer, $MgCl_2$ (2.5 mM), primers (200 nM each), and 5 U *Taq* polymerase (Invitrogen, Karlsruhe, Germany) to the RT product (final volume 50 µL). Forty-five cycles were performed (denaturation at 94°C, 25 s; annealing at 51°C, 2 min for the first 5 cycles, and 45 s for the remaining cycles; extension at 72°C, 25 s; final elongation at 72°C, 7 min). An aliquot (2 µL) of the PCR product was used as template for the second PCR (35 cycles; annealing at 54°C, first 5 cycles: 2 min, remaining cycles: 45 s) using nested primers (Table 1). The conditions were the same as described for the first round, but dNTPs (4 × 50 µM) and Platinum *Taq* polymerase (2.5 U; Invitrogen) were added. Products were identified with gel electrophoresis using a molecular weight marker (low molecular weight marker, New England Biolabs, Frankfurt, Germany). As a positive control, RT-PCR for total RNA from mouse brain were run in parallel. Negative controls were performed using distilled water or bath solution for RT-PCR. The primers for the targets were located on different exons to prevent amplification of genomic DNA.

2.10 | Immunohistochemistry

Mice were anesthetized by intraperitoneal injection of Xylaxin/Ketamin and intracardially perfused by ice cold phosphate buffer saline (PBS) followed by 4% paraformaldehyde (PFA). Brains were dissected, post fixed overnight in 4% PFA at 4°C and transferred into PBS. Coronal brain sections (40 µm thickness) were obtained with a vibratome (Leica VT1200S; Leica Microsystems) and washed three times with PBS before incubating in blocking solution (0.5% Triton-X100 and 10% normal got serum (NGS) in PBS) for 2 h at room temperature. We used the following primary antibodies (diluted in PBS with 0.1%Triton-X100 and 5%NGS, applied for at least 12 h at 4°C): chicken anti-GFP (1:500; Abcam), rabbit anti-MBP (1:250; Millipore), mouse anti-GSTpi (1:500; BD Bioscience), rabbit anti-Ki67 (1:500; Novocastra), rabbit anti-PDGFRα (1:200; Thermo Fisher). Secondary antibodies: Goat anti-chicken Alexa 488 (1:500; Thermo Fisher), goat anti-rabbit Alexa 594 (1:500; Thermo Fisher), goat anti-rabbit Alexa 647 (1:500; Thermo Fisher), goat anti-mouse Alexa 647 (1:500; Thermo Fisher) (all in PBS with 0.1%Triton-X100 and 5% NGS, 2 h at room temperature). After nuclei staining with Hoechst (Molecular Probes, 10 min, 1:100 in dH_2O) sections were washed again and mounted on cover slips (Aqua-Poly/Mount, Polyscience).

2.11 | Confocal microscopy

Images were captured with a confocal laser scanning microscope (SP8 LSM, Leica) using a 20x immersion objective (Leica). Z-stack images of 1 µm interval (total depth of 4 µm) were processed with LAS software (Leica) and analyzed with Fiji software. Images were acquired and analyzed from three hippocampal sections per mouse, from at least six animals per group. To evaluate recombination, differentiation, proliferation and myelination, the data from strata radiatum and lacunosum-moleculare were averaged, accordingly. Recombination efficiency was calculated as the proportion of cells co-expressing EYFP and PDGFRα among all $PDGFR\alpha^+$ cells. To assess changes in the differentiation of recombined (i.e., $EYFP^+$) NG2 glia cells into oligodendrocytes, sections were stained for the oligodendrocyte marker GSTpi and the proportion of cells co-expressing EYFP and GSTpi among all $EYFP^+$ cells was determined. Proliferation was quantified by calculating the ratio of cells co-expressing Ki67 and EYFP among all EYFP cells. For quantification of myelination, MBP fluorescence intensity was determined by comparing datasets obtained from slices of wild type (wt) mice with thoses of Kir4.1 ko mice.

2.12 | Expansion microscopy

The expansion microscopy (ExM) protocol for imaging proteins with conventional primary and secondary antibodies was adopted from Deshpande et al. (2017), Herde et al. (2020), and Asano et al. (2018). Fixed coronal hippocampal slices (70 µm thickness) were cut on a vibratome and blocked overnight at 4°C in blocking buffer (5% normal goat serum, 1% Triton-X100 in PBS pH 7.4). Primary antibodies were incubated in blocking buffer for 48 h at 4°C. Antibodies used were: chicken anti-GFP (1:1000; Abcam ab13970, lot: GR236651-g), rabbit anti-MBP (1:200; Millipore AB980, lot: 2869285) and mouse anti-SMI312 (1:100; Biolegend 837904, lot: B263754). After washing (PBS, 3 × 20 min, RT), secondary antibodies were incubated overnight at 4°C in blocking buffer. Secondary antibodies used were: goat anti-chicken Alexa Fluor 488 (1:200; ThermoFisher A11039, lot: 1691381), goat anti-mouse Alexa Fluor 568 (1:200; ThermoFisher A1131) and goat anti-rabbit biotin (1:200; Jackson ImmunoResearch 111-066-144). The following day, after washing (PBS, 3 × 20 min, RT), Hoechst 33342 was incubated for 10 min at RT in distilled water (1:2000). After washing (PBS, 3 × 20 min, RT), the slices were pre-imaged with 40x/1.1 NA objective in a Leica SP8 confocal microscope and a z-stack (1 µm interval) of the tip of the DG acquired for expansion factor calculation (only Hoechst 33342 signal imaged). Further treatment was adopted from Deshpande et al. (2017) and Asano et al. (2018). Briefly, slices were incubated in 1 mM methylacrylic acid-NHS for 1 h at RT. After washing (PBS, 3 × 20 min, RT), slices were incubated for 45 min at 4°C in monomer solution (in g/100 mL PBS: 8.6 sodium acrylate, 2.5 acrylamide, 0.15 *N*,*N*′-methylenebisacrylamide, 11.7 NaCl). Then, slices were incubated for 5 min at 4°C in gelling solution (monomer solution supplemented with % (w/v): 0.01 4-hydroxy-TEMPO; 0.2 TEMED; 0.2 ammonium persulfate). Slices in the gelling solution were placed on a glass slide and the preparation was covered with a coverslip and incubated for 2 h at 37°C. To ensure that all samples have the same thickness, the gel was sandwiched between a glass slide and a coverslip, with precise spacers at the edges with 170 ± 5 µm thicknesses. Coverslips and excess gel around the slice were removed after gelification and gels incubated overnight at 25°C in digestion buffer containing (50 mM Tris pH 8.0, 1 mM EDTA, 0.5% Triton-X100, 0.8 M guanidine hydrochloride, 16 U/mL of proteinase K). The following day, the digestion buffer was removed and the gels were incubated with streptavidin Alexa Fluor 647 (1:100; Jackson ImmunoResearch 016-600-084, lot: 124695) in PBS for 2 h at RT. For expansion, slices were then incubated in distilled water (adjusted pH 7.4 with NaOH) for 2.5 h at RT and water exchanged repeatedly every 15–20 min. Finally, slices were mounted on poly-lysine coated µ-Slide 2 well Ibidi-chambers and sealed with a poly-lysine coated coverslip on top, adding a drop of water to prevent the gel from drying. Ibidi chambers and coverslips were poly-lysine coated by incubation with poly-l-lysine solution (0.1% w/v in water, P8920, Sigma-Aldrich, lot: 050M4339) for at least 45 min at RT shaking and dried with pressured air. Prior to imaging the region of interest (ROI) for each slice, the tip of the DG was imaged with a 20x/0.75 NA objective (z-stack 6 µm interval with Hoechst 33342 signal only). The expansion factor was determined by identifying the same cells labeled with Hoechst 33342 in the tip of DG before and after expansion and averaging the expansion factor of 10 measures. On average, we obtained an expansion factor of 4.546 ± 0.242 ($n = 10$). ROIs were imaged on a Leica SP8 inverted confocal microscope using a 40x/1.1 NA objective and hybrid detectors. Image stacks were then deconvolved in Leica Systems software and analyzed with Fiji. 3D-Isosurfaces were constructed for MBP and SMI312 immunofluorescence using IMARIS 8.31 (Bitplane, Zurich, Switzerland) isosurface routines including intensity thresholding, background correction and minimal object volume. This set of parameters was optimizes for best-fitting result, verified by visual inspection and kept constant for all analyses. Volume, summed fluorescence intensity and fluorescence density of the individual 3D objects generated in this way were determined for four different ROIs for control and Kir4.1 ko animals. Physical xyz-voxel size (i.e., after expansion) of confocal stacks of interest was 0.284 × 0.284 × 0.8 µm^3 taken as 1024 × 1024 × 60 pixels. This corresponds to an original (i.e., before expansion) ROI size of 66.8 × 66.8 × 11 µm^3.

2.13 | Efficiency of Kir4.1 deletion

To estimate the efficiency of homologous recombination after tamoxifen injection, immunostaining for the reporter EYFP (Srinivas et al., 2001) and PDGFRα, a specific marker of NG2 glia (Rivers et al., 2008) was performed in the hippocampus (CA1 st. radiatum and st. lac. moleculare) (Figure S1A). The number of PDGFRα$^+$EYFP$^+$ cells was determined and divided by the total number of PDGFRα$^+$ cells. EYFP$^+$ cells contacting blood vessels were excluded, because they are pericytes and lack PDGFRα (Huang et al., 2014; Karram et al., 2008). Between 4 and 8 weeks after tamoxifen injection, 60%–80% of PDGFRα$^+$ cells also expressed EYFP, both in controls (i.e., mice lacking floxed Kir4.1) and Kir4.1 knockout (ko) mice (3 mice each; Figure S1A, B). This proportion (i.e., the efficiency of recombination) might have been underestimated because of the limited fluorescence intensity of recombined cells in Rosa26-EYFP reporter mice (Huang et al., 2014). Four weeks after tamoxifen treatment, the density of PDGFRα$^+$ cells was similar between control and Kir4.1 ko mice (Figure S1A, C; Table S1). In control mice, however, the density of NG2 glia decreased by about 40% both hippocampal subregions 8 weeks after tamoxifen application (Figure S1C; Table S1). These developmental changes are in line with previous data and might be attributed to a limited differentiation of NG2 glia and the increase of brain volume (Moshrefi-Ravasdjani et al., 2017; Zhang et al., 2005).

In a second approach to estimate recombination efficiency, we determined Kir4.1 mRNA in FAC sorted NG2 glia from Kir4.1 ko and control mice. The quality of fluorescence activivated cell (FAC) sorting was evaluated in parallel experiments using wt (C57BL6) mice as negative control and Kir4.1 ko mice. With the latter, we defined a sorting window by the peak of EYFP fluorescence intensity at 527 nm as depicted in the sideward scatter of the FAC sorter. The fluorescence intensity of EYFP$^+$ cells was at least 10 times higher than background

fluorescence (Figure S2A). FAC sorted NG2 cells of NG2ki-EYFP mice (Karram et al., 2008) (N = 10) were tested for cell type-specific mRNA expression (neurons, Rbfox3; microglia, Aif1; astrocytes, Aldh1L1; NG2 glia, PDGFRα). The housekeeping gene β-actin served as an internal standard. Gene expression ratios towards β-actin were determined and normalized to PDGFRα mRNA (N = 10). In FAC sorted hippocampal NG2 glia we found less than 2% of mRNAs coding for other cell types (Rbfox3, 0.79 ± 0.52%; Aif1, 1.11 ± 0.71%; AldH1L1, 0.12 ± 0.07%), confirming the high specificity of our FACS approach (Figure S2B). Kir4.1 mRNA was determined in recombined cells from the hippocampus of Kir4.1 ko and control mice, 3 weeks after tamoxifen. Threshold cycle differences, ΔC_T, between Kir4.1 and β-actin were determined in individual samples and the gene ratio Kir4.1/β-actin was calculated (Equation 1). In recombined NG2 glia of control mice the gene ratio was 0.102 ± 0.012 (N = 11), while in Kir4.1 ko mice, the ratio was 0.0136 ± 0.0049 (N = 8), i.e. 87% lower than in the controls (Figure S2 C). The Kir4.1 mRNA amount in hippocampal NG2 cells from the NG2ki-EYFP mouse line was similar to recombined control cells in the hippocampus of NGCEcreERT2 mice (not shown).

2.14 | Statistics

Data were analyzed with Igor Pro (WaveMetrics), (R Core Team (2020)) and Origin (OriginLab) software. All data were tested for normal (Gaussian) distribution (Shapiro–Wilk test or Lilliefors test, dependent on the number of data points), followed by two sampled Student's t or Mann–Whitney U test with or without Welch correction for equal or differing variances. For multiple group analysis data were tested with Kruskal–Wallis ANOVA followed by Dunn's test, 1-way ANOVA followed by Tukey test or 2-way ANOVA followed by Bonferronis *t*-test. Significance level was set to $P < .05$. Non-Gaussian distributed data are displayed in Tukey box plots showing median (central line), quartiles (25% and 75%; box) and whiskers (± 1.5 times the interquartile range). Extreme outliers outside of the 3* interquantile range (IQR) fence were removed. Outliers are shown as dots. For the analysis of the distribution of ePSC parameters, a density estimator with a Gaussian kernel was used. We used the sm package of R for this purpose.

3 | RESULTS

3.1 | Mice with Kir4.1 deficient NG2 glia show improved novel object location recognition

To figure out whether and how dysfunctional NG2 glia affects mouse behavior, we studied memory performance of mice with selectively ablated Kir4.1 in NG2 glia. Firstly, we assessed spatial working memory of the animals using the Y-maze test, where the ratio of alternations correlates with the strength of working memory. The genotype did not influence the behavior of the mice in this paradigm (Figure 1a). Testing novel object location recognition (NOLR) is a sensitive tool to evaluate spatial memory. Animals, which remember the original location of an object spend more time investigating the object in a new position, thus showing novelty preference. Notably, testing for novelty preference values indicated a significantly improved recognition ability of Kir4.1 ko mice ($p = .016$) (Figure 1b). Finally, to test social memory, we applied a partner recognition test. Similar to the novel object location recognition test, a positive novelty preference value is an indicator of recognition. At none of the tested inter-trial intervals we found a significant influence of the genotype on social memory

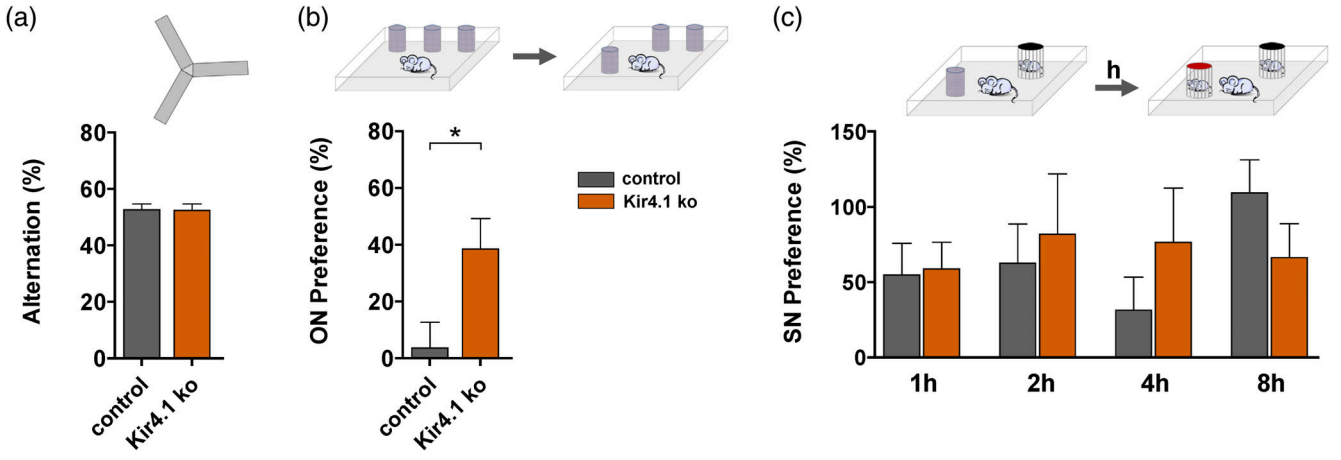

FIGURE 1 NG2 glia-specific deletion of Kir4.1 improves performance in new object location recognition. (a) Working memory was tested in a Y-maze paradigm. Genetic deletion of Kir4.1 did not influence spatial working memory as the proportion of alternation was not significant between Kir4.1 ko and control mice (control, $N = 17$; Kir4.1 ko mice, $N = 19$). (b) Novel object location recognition test. Object novelty (ON) preference, an indicator of spatial memory, was significantly higher in Kir4.1 ko mice (38.50 ± 10.34%, $N = 14$) than in control mice (3.66 ± 8.69%, $N = 14$). (c) Partner recognition test. Novelty preference as an indicator of social memory was tested at different inter-trial times (1 h, 2 h, 4 h, and 8 h). No difference in social novelty (SN) was detected between Kir4.1 ko (N = 19) and control mice ($N = 16$). 2-way ANOVA with Tukey HSD. Mean ± SEM. Asterisk indicates statistically significant difference (*$p < .05$).

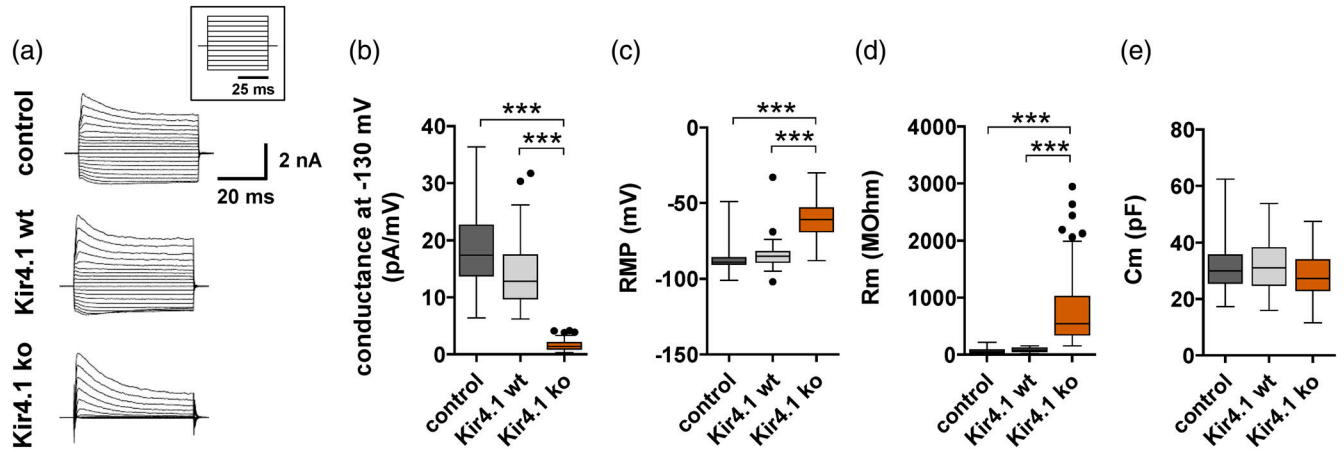

FIGURE 2 *Kir4.1 channels determine passive membrane properties of hippocampal NG2 glia*. (a) Examples of whole-cell current pattern of recombined NG2 glia cells in control and Kir4.1 ko mice evoked by de- and hyperpolarizing steps between −160 mV and + 20 mV lasting for 50 ms. (b) Cells with a conductances <6 pA/mV at −130 mV were identified as Kir4.1 knockout (ko) cells (median Kir4.1 ko cells: 1.4 pA/mV, $n = 128$, and $N = 17$). NG2 glia of Kir4.1 ko mice that still expressed Kir4.1 currents were termed Kir4.1 wt cells (median: 12.8 pA/mV, $n = 55$, and $N = 15$). The membrane conductance of Kir4.1 wt cells resembled that of NG2 glia of control mice (median 17.4 pA/mV, $n = 82$, and $N = 9$). (c) In the absence of Kir4.1 the membrane potential of NG2 glia was depolarized to −61 mV compared to Kir4.1 wt (−85 mV) and control cells (−89 mV). (d) The membrane resistance in cells lacking Kir4.1 (546 MΩ) was much higher than in Kir4.1 wt (81.2 MΩ) and control cells (50.8 MΩ). (e) The membrane capacitance was not affected by deletion of Kir4.1 (median Kir4.1 ko cells, 27.3 pF; Kir4.1 wt cells, 31.1 pF; control cells, 30.0 pF). Kruskal-Wallis ANOVA with Dunn's test. Asterisks indicate statistically significant differences (***$p < .001$).

(Figure 1c). Thus, NG2 glia-specific deletion of Kir4.1 improves spatial memory. These results suggest that deletion of Kir4.1 did not lead to a generally improved learning and memory, because working memory or social declarative memory remained unchanged in the Kir4.1 ko mice.

3.2 | A vast majority of recombined NG2 glial cells in the hippocampus lack Kir4.1 channels

Since the hippocampus is involved in the formation of spatial memory, we performed further analyses to characterize the properties of NG2 glia in this brain region. Patch-clamp recordings were performed 3–4 weeks after tamoxifen injection (Figure 2). $EYFP^+$ (i.e., recombined) cells were selected in the CA1 stratum radiatum of control ($n = 82$ cells, $N = 9$ mice) and Kir4.1 ko mice ($n = 183$, $N = 17$) and tested for the presence of Kir currents. Unexpectedly, in Kir4.1 ko mice two populations of fluorescent cells co-existed in the same slices, either still expressing (termed Kir4.1 wt cells) or lacking Kir currents (membrane conductance at −130 mV, <6 pA/mV; termed Kir4.1 ko cells) (Figure 2a,b). Compared to $EYFP^+$ cells from control mice and Kir4.1 wt cells, which had resting potentials close to the K^+ equilibrium potential and a membrane resistance of 50.8–81.2 MΩ, Kir4.1 ko cells were dramatically altered in their passive membrane properties. These cells lacking Kir4.1 were characterized by depolarized resting potentials and a drastically increased input resistance, while membrane capacitance was unaffected (Figure 2 c–e).

To confirm the presence or absence of Kir4.1 mRNA in recombined NG2 glial cells with or without Kir currents, subsequent to patch clamp recording we harvested the cytoplasm of single fluorescent cells from the CA1 region of Kir4.1 ko mice. In cells without inward currents (Kir4.1 ko), Kir4.1 transcript was always absent ($n = 15$) while cells with inward currents (Kir4.1 wt) still expressed Kir4.1 mRNA (7/8 cells; Figure S2 D). To test for functional expression of Kir4.1, Ba^{2+} (100 μM) was applied (focal pressure application). In control cells, the membrane (chord) conductance decreased by almost 90% in Ba^{2+} solution, and similar Ba^{2+} sensitivity was found in Kir4.1 wt cells (Figure S2E, F). Notably, even in Kir4.1 ko cells the residual inward currents were Ba^{2+}-sensitive (Figure S2 G), which might suggest that part of the inward currents in NG2 glia were mediated by channels other than Kir4.1 (Albrecht et al., 2019; Chan et al., 2013).

Together, these experiments revealed that in the hippocampus of Kir4.1 ko mice, tamoxifen-induced recombination led to the deletion of Kir4.1 channels in a majority of NG2 glial cells.

3.3 | Increased excitability of Kir4.1 deficient hippocampal NG2 glial cells

Immature dentate granule cells (DGCs) express Kir channels at a lower density than mature DGCs, resulting in a higher input resistance and increased excitability upon synaptic input of the former (Mongiat et al., 2009). To test if Kir4.1 similarly determines input resistance and excitability of NG2 glial cells in the hippocampus, mPSPs were recorded in the presence of TTX (0.5 μM). Indeed, mPSP amplitudes, rise and decay time constants in Kir4.1 ko cells significantly exceeded those of cells expressing Kir4.1 (Figure 3 a–d), which resembled changes seen when pharmacologically blocking Kir4.1 channels in NG2 glia (Chan et al., 2013). Upon unitary quantal release, depolarizations of about 1.8 mV were detected in cells lacking Kir4.1, responses

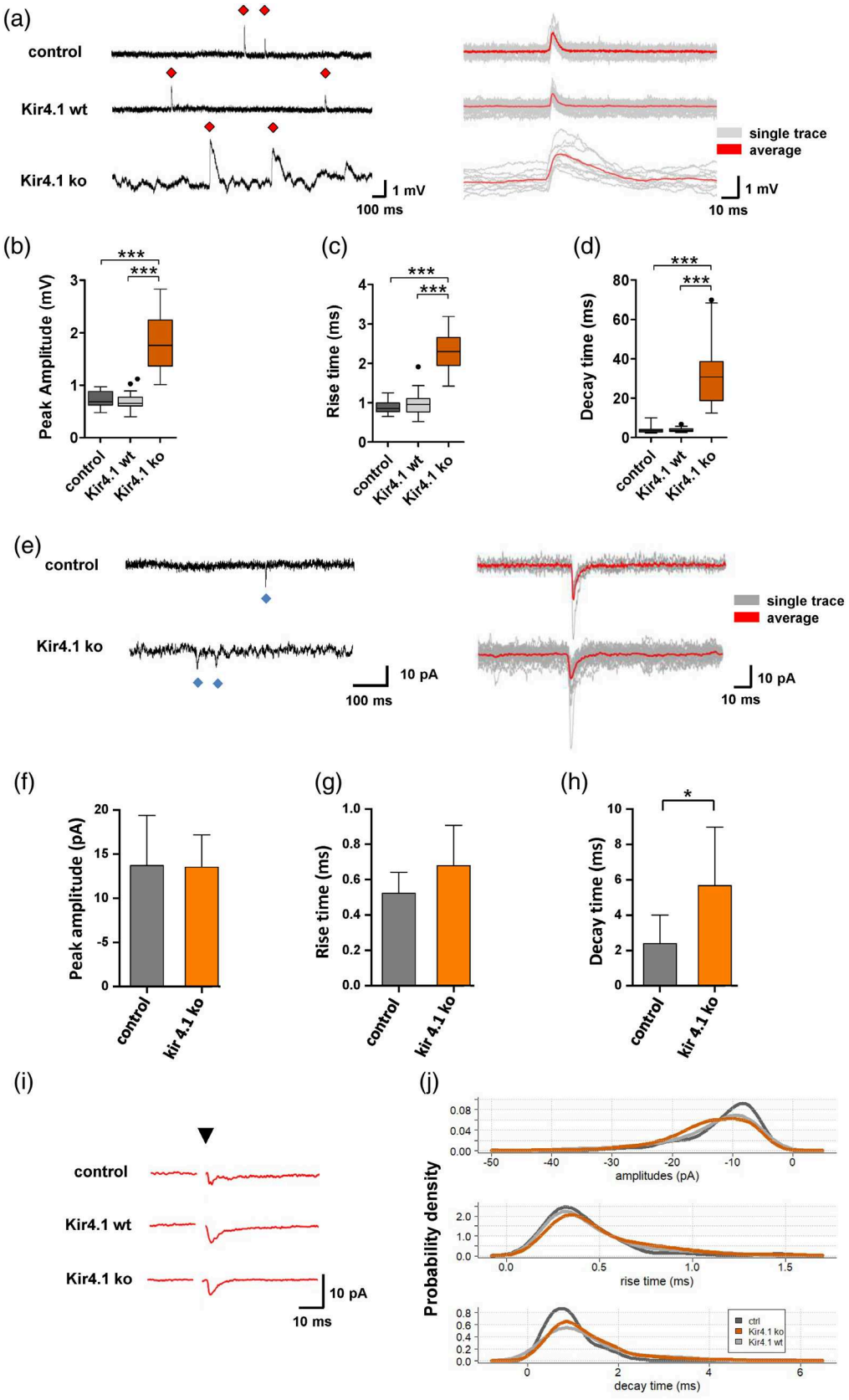

FIGURE 3 Legend on next page.

that were more than doubled compared to control and Kir4.1 wt cells (Figure 3b). These depolarizations lasted several tens of ms in Kir4.1 ko cells while in cells still expressing Kir4.1, mPSPs declined to zero within 10 ms (Figure 3a, d). Similarly, a slowdown of the rise time constant was observed in cells devoid of Kir4.1 (Figure 3c). Together, these observations indicated that in NG2 glia, Kir4.1 critically determines membrane resistance and responsiveness to neuronal input.

Both glutamatergic and GABAergic input depolarizes hippocampal NG2 glia (Jabs et al., 2005; Lin & Bergles, 2004; Passlick et al., 2013). To isolate glutamatergic from GABAergic input, the bath solution was supplemented with the $GABA_AR$ blocker picrotoxin (150 μM). Peak amplitude and kinetics (rise time and decay time) of mPSPs were not affected by the blocker (Figure S3 A–C; Table S2). Co-application of picrotoxin and NBQX (10 μM), a blocker of AMPA/kainate receptors, fully abolished mPSPs (not shown).

Next we tested whether mPSCs were affected in cells lacking Kir4.1. Unitary amplitude and rise time were similar in control and Kir 4.1 ko cells, while decay times of mPSCs were prolonged in Kir 4.1 ko NG2 glia (Figure 3 e–h). Minimal stimulation of Schaffer collaterals was applied to test whether deletion of Kir4.1 in NG2 glia also affects evoked postsynaptic currents (ePSCs) (Figure 3i). In Kir4.1 ko cells rise time, decay time and amplitudes of the ePSCs increased to 138, 228 and 161%, respectively (Table 2 b). In the presence of picrotoxin (150 μM), similar changes were found (rise time, decay time and amplitudes, increase to 121, 119 and 134%, respectively; see Table 2 b for details). The probability density functions of the ePSC parameters, representing a measure of the scaled (integral over the curve is 1) frequency of their respective occurrence, were shifted towards higher excitability of Kir 4.1 ko cells (Figure 3j). For example, in Kir4.1 ko mice, more cells with higher ePSC amplitudes occurred, leading to a left shift of the orange curve. Thus, deletion of Kir4.1 entailed an increased excitability of hippocampal NG2 glia.

3.4 | Impaired LTP in mice with Kir4.1 deficient NG2 glia is rescued by stimulating TrkB receptors

To test whether the increased responsiveness of NG2 glia in the hippocampus of Kir4.1 ko mice affects neuronal signaling, fEPSPs were recorded in the stratum radiatum of the CA1 region upon stimulation of the Schaffer collaterals (Figure 4a). Basal excitability in the hippocampus was similar in control and Kir4.1 ko mice as judged by the unchanged input–output curves and by stimulus intensities required to evoke half-maximum fEPSP amplitudes (Figure S4A, B). Next we investigated long-term potentiation (LTP) of transmission at Schaffer collateral - CA1 pyramidal cell synapses. A standard theta burst protocol was used to induce LTP in slices of control (pooled NG2-YFP and tamoxifen-injected NG2creERT2 mice) and Kir4.1 ko mice. We noted reduced post tetanic potentiation (1–3 min after TBS, by 23.4%) and LTP (25–30 min after TBS, by 19.5%) in slices obtained from Kir4.1 ko mice (Figure 4 b, c), indicating that NG2 glial cells influence neuronal plasticity. This effect was not caused by changes in presynaptic release probability because the paired pulse ratios before and after LTP induction were similar in control and Kir4.1 ko mice (Figure 4 d, e). Since the neurotrophin BDNF is critically involved in hippocampal LTP induction (Korte et al., 1995; Minichiello et al., 1999;Chen, Huang, et al., 1999) we tested whether stimulation of the TrkB receptor might rescue the loss of LTP observed in Kir4.1 ko mice. The high-affinity TrkB receptor agonist, 7,8-DHF, was reported to mimic BDNF actions such as receptor dimerization and phosphorylation as well as activation of downstream signaling cascades (Jang et al., 2010). Indeed, incubation of slices from Kir4.1 ko mice in 7,8-DHF (1 μM, 50 min) prior to TBS completely rescued LTP (1–3 min after TBS, to 97.2% of the control; 25–30 min after TBS, to 100.2% of the control) (Figure 4 f, g) while 7,8-DHF did not affect LTP in slices from control mice vs. untreated controls (to 98.6% and to 103.4%, 1–3 min and 25–30 min after TBS, respectively). Neither in control nor in Kir4.1 ko mice, the TrkB-receptor agonist influenced input–output relation or paired-pulse ratio (Table S3). These data indicate a role for NG2 glia in BDNF–TrkB receptor mediated LTP induction in the hippocampus.

3.5 | Proliferation and differentiation of hippocampal NG2 glia are only slightly affected after deletion of Kir4.1

To clarify whether inducible deletion of Kir4.1 in NG2 glial cells affects their proliferation or differentiation, immunohistochemical

FIGURE 3 Increased amplitude and prolonged kinetics of mPSPs, mPSCs and ePSCs in hippocampal NG2 glial cells lacking Kir4.1. (a) Left: Example traces of mPSPs of control (top), Kir4.1 wt (middle) and Kir4.1 ko (bottom) NG2 glia cells. Red diamonds indicate individual events. Right: Corresponding superimposed single (gray) and average mPSP traces (red; average of 10–29 events). (b) In Kir4.1 ko cells, peak mPSPs ($n = 27$, $N = 15$) were more than twice as high as in control ($n = 13$, N = 7) and Kir4.1 wt cells ($n = 22$, $N = 12$). (c, d). Rise and decay time of mPSPs in Kir4.1 ko cells were significantly prolonged. Box plots show median (central line), quartiles (25% and 75%) and whiskers (±1.5 times the interquartile range). Asterisks indicate statistically significant differences (*t*-test, ***$p < .001$). E) Left: Sample traces of mPSCs from NG2 glia of control and Kir4.1 flox mice. Blue diamonds indicate individual events. Right: Corresponding superimposed single (gray) and average mPSC traces (red; average of 6 and 20 events, respectively). (f) Average peak amplitude of mPSCs recorded from control (−13.7 ± 5.7 pA) and Kir 4.1 ko cells (−13.5 ± 3.6 pA; *t*-test, $p = .95$). (g, h) Kinetics of mPSCs in control and Kir4.1 ko cells (rise time: 0.52 ± 0.11 vs. 0.68 ± 0.23 ms, t-test, p = 0.14; decay time: 2.38 ± 1.62 vs. 5.67 ± 3.31 ms (t-test, * p = 0.036). Data were taken from 7 cells, $N = 3$ for each genotype. Holding potential in control and Kir4.1 ko cells: −80 and − 60 mV, respectively. (i) Averaged time course of NG2 glia eEPSCs upon stimulation of Schaffer collaterals. Stimulation pulse is indicated by black triangle. (j) Probability density functions of amplitudes, rise and decay times of ePSCs in the presence of picrotoxin (150 μM). Number of control and Kir4.1 ko mice, N = 5 and 8. See Table 2 for further details.

TABLE 2 Properties of mPSPs (a) and ePSCs (b) of control, Kir4.1 wt and Kir4.1 ko cells.

(a)	ACSF		
	Control	**Kir4.1 wt**	**Kir4.1 ko**
Amplitude (mV)	0.69	0.65	1.76
	(0.62–0.88)	(0.61–0.77)	(1.37–2.24)
	Kir4.1 ko	*< 2 E-16*	–
	control	0.96	*< 2 E-16*
	ANOVA		*p < 2 E-16*
Rise time (ms)	0.85	0.95	2.30
	(0.77–0.99)	(0.76–1.11)	(1.94–2.66)
	Kir4.1 ko	*2E-09*	–
	control	0.7	*3E-08*
	Kruskal–Wallis		*p = 3E-10*
Decay time (ms)	3.49	3.68	30.84
	(2.80–4.18)	(3.11–4.40)	(18.80–38.68)
	Kir4.1 ko	*7 E-09*	–
	control	0.86	*1 E-08*
	Kruskal–Wallis		*p = 2 E-10*
Cells	13	22	27

(b)	ACSF			+ PicTx		
	Control	**Kir4.1 wt**	**Kir4.1 ko**	**Control**	**Kir4.1 wt**	**Kir4.1 ko**
Amplitude (pA)	11.2	18.0	18.1	9.5	11.1	12.8
	(6.8–16.3)	(11.3–25.1)	(12.0–25.9)	(7.5–13.2)	(8.2–16.5)	(8.8–16.7)
	[68]	[212]	[491]	[87]	[171]	[227]
	Kir4.1 ko	0.23	–	*Kir4.1 ko*	0.17	–
	control	*2E-06*	*5E-09*	*control*	0.12	*6E-03*
	Kruskal–Wallis		*p = 1E-08*	*Kruskal–Wallis*		*p = 8E-03*
Rise time (ms)	0.34	0.42	0.47	0.34	0.37	0.41
	(0.27–0.41)	(0.34–0.54)	(0.36–0.61)	(0.28–0.49)	(0.28–0.55)	(0.31–0.61)
	[54]	[173]	[362]	[80]	[154]	[196]
	Kir4.1 ko	*6E-04*	–	*Kir4.1 ko*	0.09	–
	control	*2E-02*	*2E-07*	*control*	0.31	0.02
	Kruskal–Wallis		*p = 2E-07*	*Kruskal–Wallis*		*p = .01*
Decay time (ms)	0.71	1.66	1.62	0.86	1.04	1.02
	(0.43–1.39)	(0.92–2.82)	(1.09–2.48)	(0.56–1.07)	(0.64–1.57)	(0.73–1.61)
	[59]	[181]	[423]	[78]	[159]	[213]
	Kir4.1 ko	*7E-09*	–	*Kir4.1 ko*	0.51	–
	control	0.79	*2E-10*	*control*	*7E-03*	*1E-03*
	Kruskal–Wallis		*p = 3E-10*	*Kruskal–Wallis*		*p = 1E-03*
Cells	4	12	6	5	7	8

Note: Data are given as median and interquartile range (quartile 25% – quartile 75%), number of measures in square brackets (b).

analysis of the proliferation marker Ki67 and a marker for mature oligodendrocytes, GSTpi, was combined with molecular analysis. Recombined EYFP$^+$ NG2 glia were identified with an GFP antibody. In st. radiatum and st. lacunosum-moleculare of the hippocampal CA1 region, only few Ki67$^+$EYFP$^+$ cells were found 8 weeks post injection (wpi; <10% of all recombined cells), and there was no difference between control and Kir4.1 ko mice (Figure 5 a, b; Table S4). In control animals, however, the total density of Ki67$^+$ cells in the st. lacunosum-moleculare was more than twice as high as in the radiatum, and deletion of Kir4.1 in NG2 glia induced an increase in total Ki67$^+$ cell density in the st. radiatum (Figure 5c, Table S4).

Next, immunostaining against gluthathione S-transferase pi (GSTpi), an enzyme expressed by oligodendrocytes (Tansey et al., 1991) was performed to test for enhanced NG2 glia differentiation after targeted Kir4.1 deletion. Control stainings using NG2ki-EYFP mice (Karram et al., 2008) confirmed the absence of GSTpi expression in EYFP$^+$ NG2 glia of the hippocampus (not shown). Eight wpi, 5%–37% of all recombined NG2 glial cells in the hippocampus of control and Kir4.1 ko mice were positive for GSTpi. Targeted deletion of Kir4.1 neither affected the number of GSTpi$^+$EYFP$^+$ cells (Figure 5 d, e; Table S4) nor the density of GSTpi$^+$ cells in these layers (Figure 5

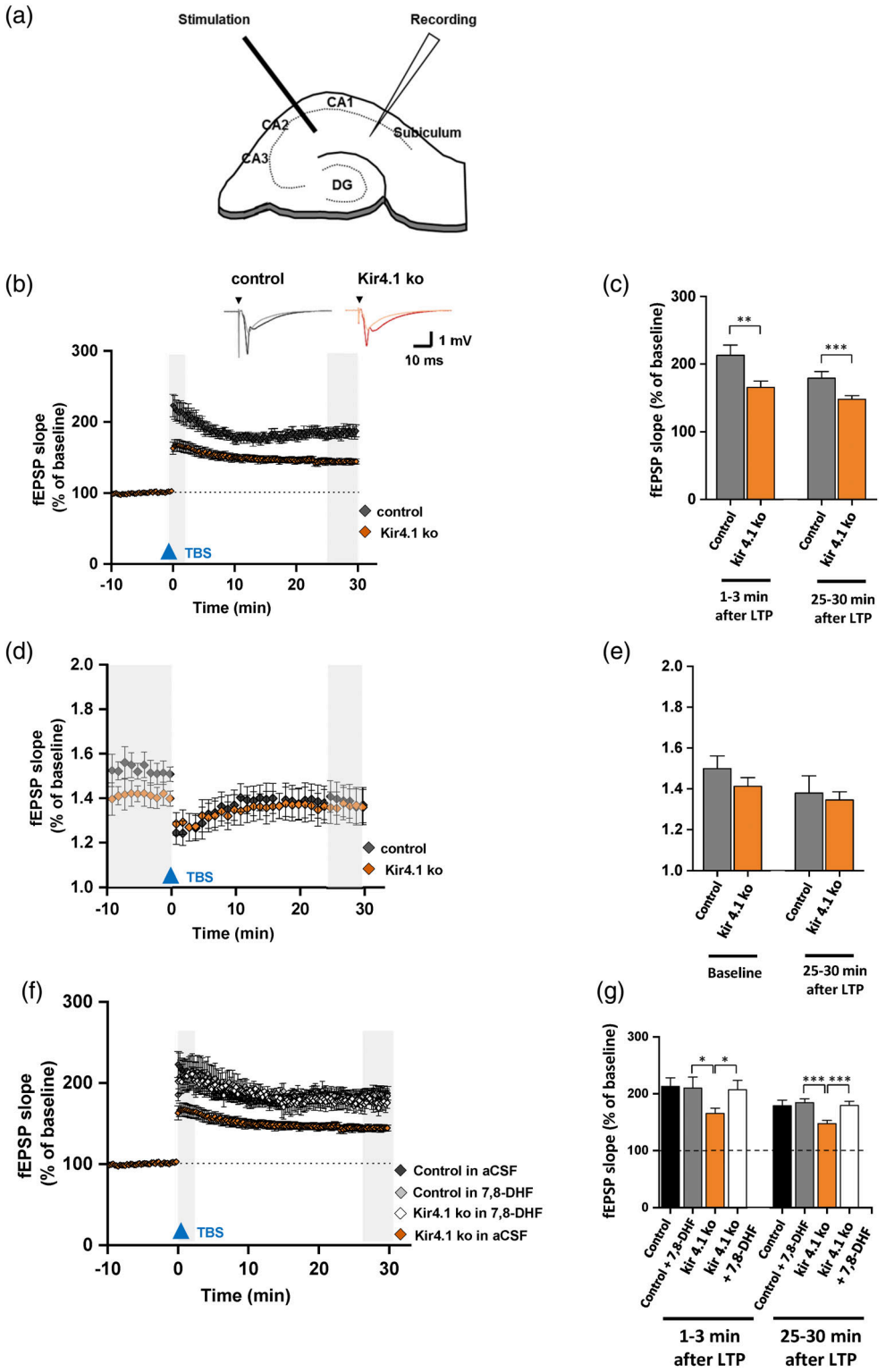

FIGURE 4 Legend on next page.

f). Thus, postnatal deletion of Kir4.1 in NG2 glia provoked no or only subtle changes in the proliferation or differentiation of those cells in the hippocampus.

3.6 | Increase of myelin-specific gene transcripts and protein in the hippocampus of Kir4.1 ko mice

Although gray matter NG2 glial cells do not form myelin or express myelin-related protein (Diers-Fenger et al., 2001), they do express corresponding transcripts, for example, for myelin-associated glycoprotein (MAG), myelin basic protein (MBP) or 2,3-cyclic nucleotide 3-phosphodiesterase (CNP) (Moshrefi-Ravasdjani et al., 2017; Ye et al., 2003). In this study, we wondered if targeted deletion of Kir4.1 in NG2 glia affects expression of MAG and MBP mRNA in FAC sorted cells. Three wpi, the MAG-to-β-actin expression ratio in hippocampi of control and Kir4.1 ko mice was 1.15 ± 0.17 and 1.69 ± 0.11. Similarly, the ratio of MBP-to-β-actin mRNA expression in control mice (2.32 ± 0.42) was lower than after Kir4.1 deletion (5.04 ± 0.44) (Figure 6a). These gene expression data were further confirmed by immunostainings for MBP in Kir4.1 ko mice. In line with the transcript data, 8 wpi strongly elevated MBP levels were observed in both hippocampal layers in Kir4.1 ko vs. control mice (st. radiatum, 0.542 ± 0.312 vs. 0.173 ± 0.14; st. lacunosum-moleculare, 6.96 ± 3.68 vs. 2.76 ± 1.68) (Figure 6 b, c).

To get further insight as to how targeted deletion of Kir4.1 affects myelination, axons and myelin sheaths were stained with antibodies against SMI312 and MBP and analyzed at higher spatial resolution using expansion microscopy (Chen et al., 2015; Chozinski et al., 2016). Analysis was confined to the st. lacunosum-moleculare because of the high MBP immunoreactivity seen in this layer (Figure 6 b, c). Based on immunostaining, 3D isosurfaces of axons (SMI312) and myelin sheaths (MBP) were constructed, further referred to as particles (Figure 6d). For MBP particles, we calculated volume, total fluorescence intensity and the density of fluorescence intensity. In Kir4.1 ko mice, in all individual ROIs placed into st. lacunosum-moleculare (Figure 6e, right) a reduction in MBP volume (decrease of the averaged medians to 74 ± 36%, $p = .02$) was found while cumulative MBP fluorescence intensity did not change ($p = .09$) (not shown). Notably, the cumulative fluorescence density of MBP particles was almost doubled in all individual ROIs in Kir4.1 ko vs. control mice (increase of the averaged medians to 192 ± 34%, $p < .001$) (averages per ROI are shown in Figure 6e left). Removing all data outliers (± 1.5 IQR) did not alter the effect size of fluorescence density (189 ± 34%, $p < .001$). In conclusion, these data indicate a significant increase in MBP density within the myelin sheaths in the hippocampus of Kir4.1 ko mice.

4 | DISCUSSION

4.1 | Deletion of Kir4.1 in NG2 glia entails changes in spatial memory

To better understand the physiological impact of NG2 glial cells in the brain, we have generated a mouse line specifically lacking Kir4.1, an inwardly rectifying K^+ channel expressed exclusively in glial cells in the central nervous system. These mice showed altered behavior, indicating disturbed function of the hippocampus. Notably, an improved performance in the NOLR test was observed, while no differences were found in Y-maze or partner recognition paradigms. At the first sight, these findings are surprising, because these models reflect different aspects of declarative memory. This memory type, tested using the partner recognition test, answers the question "what or who". Y-maze test result shows the strength of short term (working) spatial memory, answering the question "where", whereas in the NOLR test we test a sub-form of declarative memory – episodic memory - "what is where". Although the hippocampus along with the medial temporal lobe including perirhinal, entorhinal and parahippocampal cortices is critical for these memory forms (Squire & Dede, 2015), there are substantial differences as to how the hippocampus and associated cortical areas contribute to them. A crucial aspect of the performance of mice in the Y-maze test is the level of the spontaneous alternations. It is not only dependent on an intact hippocampus (Phillmore & Klein, 2019), but also on the integrity of limbic and non-limbic pathways (Lalonde, 2002). This model is based on the strength of working memory of mice and in addition to hippocampus, the prefrontal

FIGURE 4 TBS-induced LTP is impaired in mice with NG2 glia-specific Kir4.1 deficiency and rescued by 7,8-DHF. (a) Position of stimulation and recording electrodes in hippocampal slices during field potential recording. (b) Time course of normalized fEPSP slopes of control ($n = 14$ slices, $N = 5$) and Kir4.1 ko mice ($n = 39$, $N = 15$) before and after induction of LTP by 3 trains of theta-burst stimulation (TBS, blue triangle). Insets show representative fEPSPs from control and Kir4.1 ko mice (before TBS, gray and orange; 25–30 min after TBS, black and red). Stimulation pulse is indicated by black triangles. (c) Post-tetanic potentiation and LTP was impaired in hippocampal slices from Kir4.1 ko mice, 1–3 min and 25–30 min after TBS (1–3 min: 163.11 ± 8.15% vs 212.81 ± 15.32%, two-sample *t*-test, $p = .007$; 25–30 min: 178.93 ± 9.96 vs. 144.01 ± 3.98, two-sample *t*-test $p = .0009$). (d) Time course of the paired pulse ratio (PPR) of control ($n = 14$, $N = 5$) and Kir4.1 ko mice ($n = 33$, $N = 12$). E) PPR was not affected in Kir 4.1 ko mice, neither before (1.50 ± 0.07 vs. 1.41 ± 0.04, two-sample *t*-test) nor 25–30 min after TBS-induced LTP (1.37 ± 0.08 vs. 1.36 ± 0.04, two-sample *t*-test). (f) Time course of normalized fEPSP slopes of control and Kir 4.1 ko slices perfused with aCSF or 7,8-DHF (1 μM in aCSF). TBS: Theta burst stimulation. (g) Analysis of the fEPSP slopes at two time points (1–3 min after TBS and 25–30 min after TBS). Statistical significance was assessed with two-sample *t*-test. At both time points, potentiation was reduced in Kir 4.1 ko slices in aCSF ($n = 39$, $N = 15$) compared to Kir 4.1 ko slices perfused with 7,8-DHF (1–3 min: 163.11 ± 8.15 vs. 206.97 ± 16.44%, $p = .02$; 25–30 min: 144.02 ± 3.98 vs. 179.36 ± 7.37%, $p = .0007$; $n = 10$, and $N = 4$) or to 7,8-DHF-treated controls (1–3 min: 209.80 ± 19.50%, $p = 0.02$; 25–30 min: 184.37 ± 6.90%, $p = .0001$; $n = 9$, and $N = 4$). Differences between controls in aCSF and 7,8-DHF were not significant (1–3 min: $p = 0.90$; 25–30 min: two-sample *t*-test, $p = .68$). Mean ± SEM.

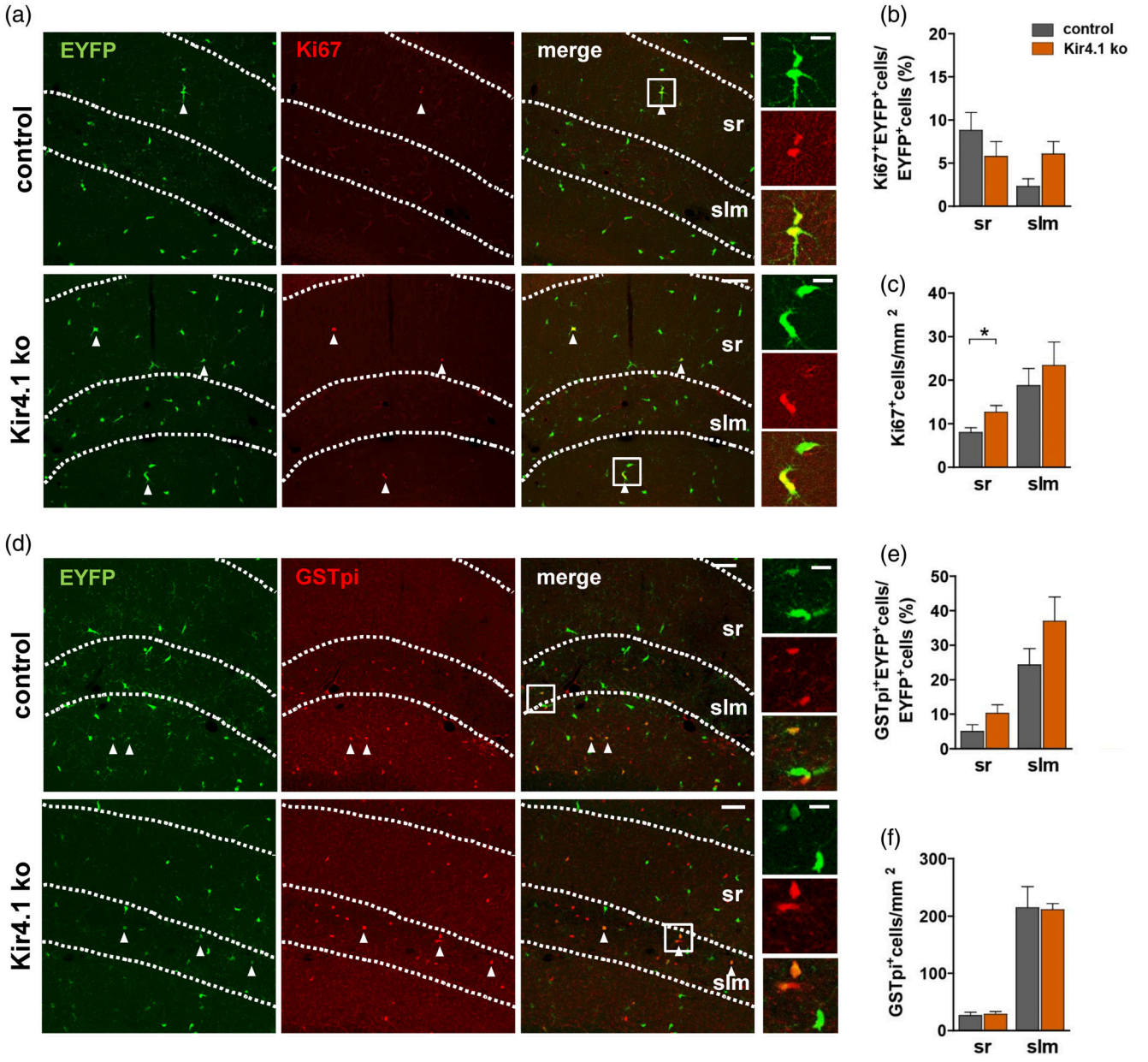

FIGURE 5 Proliferation and differentiation of hippocampal NG2 glia remained largely unaffected in Kir4.1 ko mice. (a) Hippocampal sections from control and Kir4.1 ko mice were immunostained with EYFP (green) and Ki67 (red). $EYFP^+Ki67^+$ cells are indicated by arrowheads. Boxed areas are given at higher resolution to the right. Scale bar 60 and 15 μm (insets). (b) The proportion of $Ki67^+EYFP^+$ cells among all $EYFP^+$ cells was similar in control and Kir4.1 ko mice. In control mice, the rate of NG2 glia proliferation in the st. radiatumr was higher than in the st. lacunosum-moleculare ($p = .037$). (c) In the st. radiatum of Kir4.1 ko mice the density of $Ki67^+$ cells was higher than in the controls (12.60 ± 1.47 vs. 8.0 ± 1.04, $p = .038$). Within the control group, the density of proliferating cells in the st. lacunosum-moleculare was higher than in the st. radiatum ($p = .038$). D) Sections were immunostained with EYFP (green) and GSTpi (red). $EYFP^+GSTpi^+$ cells are indicated by arrowheads. Boxed areas are shown at higher resolution to the right. Scale bars 60 and 15 μm (insets). E). The proportion of recombined NG2 glia ($EYFP^+$) differentiating into oligodendrocytes ($EYFP^+GSTpi^+$) did not differ between genotypes. However, layer-specific differences were found (st. radiatum vs. st. lacunosum: Kir4.1 ko, p = .003; control, $p = .04$). (f) The density of $GSTpi^+$ cells was not different between control and Kir4.1 ko mice. However, in both genotypes higher values were observed in the st. lacunosum-moleculare versus st. radiatum (control, $p < .001$; Kir4.1 ko, $p < .001$). Significant differences between control and Kir4.1 ko mice are indicated by asterisks (*$p < .05$; Mann–Whitney U Test). For the sake of clarity, layer-specific differences are not marked. Mean ± SEM. Number of mice is given in bar graphs. For further details see Table S3. sr, st. radiatum; slm, st. lacunosum-moleculare.

cortex also significantly contributes (Albayram et al., 2016; Lynch et al., 2004). The dorsal hippocampus plays an irreplaceable role both in partner recognition and NOLR, but specifically the CA2 region in the former (Wersinger et al., 2002) and the CA1 region in the latter (Larkin et al., 2014). The peculiarity of the NOLR paradigm demonstrates also that performance in this test is especially sensitive to

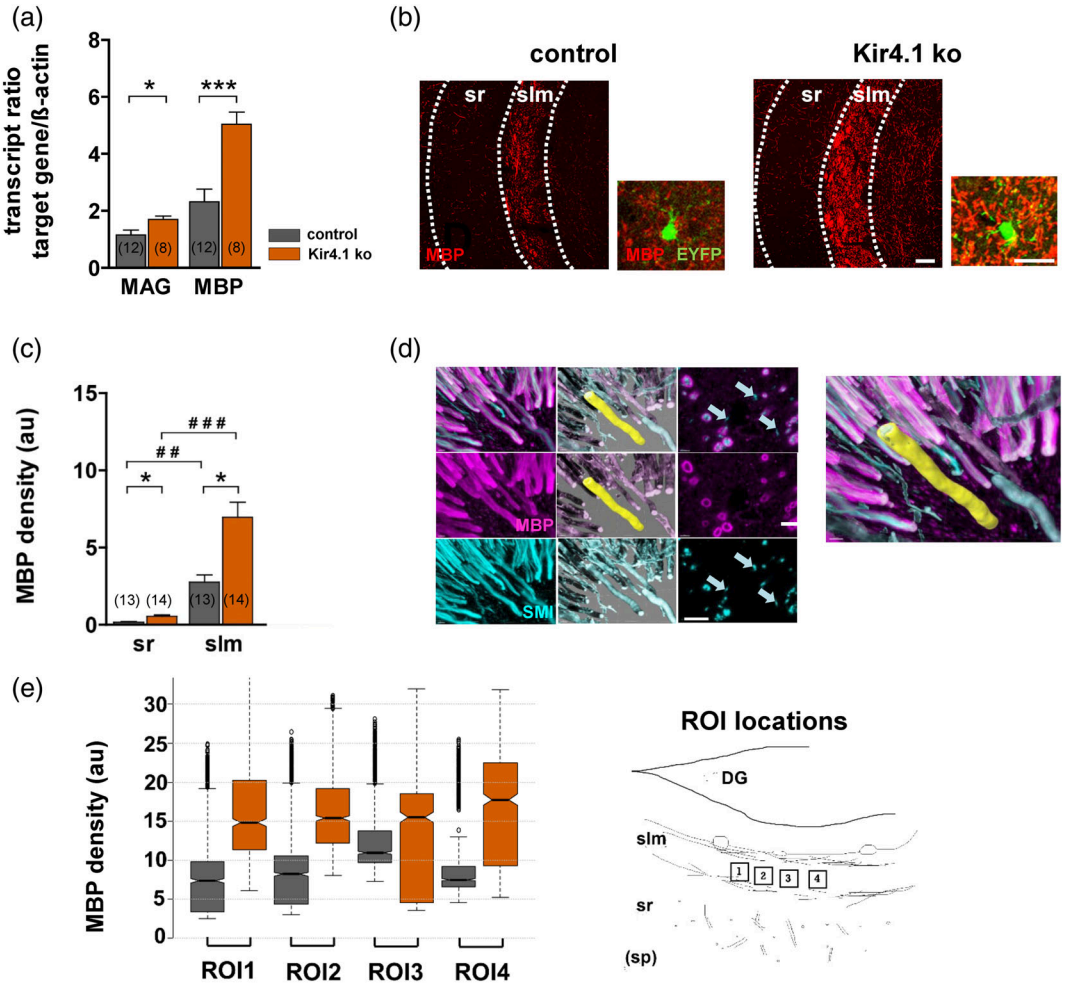

FIGURE 6 Enhanced MBP expression in the hippocampus of mice with NG2 glia-specific deletion of Kir4.1. (a) Transcript analysis of FACsorted recombined NG2 glia revealed a significant upregulation of MAG (*p < .05; t-test) and MBP (***p < .001; t-test) in Kir4.1 ko ($N = 8$) vs. control mice ($N = 12$). (b) Hippocampal sections from control and Kir4.1 ko mice were immunostained for MBP (red). Blowups show recombined NG2 glial cells (EYFP$^+$) expressing MBP. Scale bars, 50 and 15 µm (blowups). (c) MBP immunoreactivity was determined as fluorescent intensity per area (density) in slices from control ($n = 37$, $N = 14$) and Kir4.1 ko mice ($n = 41$, $N = 14$). Location and genotype were significantly different for the parameter MBP density. In both, Kir4.1 ko and control mice, maximal values were observed in the st. lacunosum-moleculare. Genotype-specific differences are indicated by asterisks, differences between layers within one genotype by hash tags (2-way 2 × 2 ANOVA followed by paired comparisons with Bonferroni adjustment) (*p < .05; $^{\#\#}p$ < .01; $^{\#\#\#}p$ < .001). (d) Subcellular analysis of MBP and SMI expression revealed by expansion microscopy. 3D representations of immunolabeling against myelin sheaths (MBP, purple), axons (SMI, turquoise) and computer-engineered matched volumes constructed by isosurfaces (semitransparent layers of the same color). The yellow structure is one exemplary highlighted MBP volume. Note the shape of a hollow cylinder. Shown are 3D visualizations (cavalier projections, 14.5 × 10.3 × 11 µm^3) of immunofluorescence (left column) and fitted isosurfaces (middle). The right column displays one single xy-plane taken from the corresponding confocal picture stack of immunostainings. The top row depicts the overlay of MBP and SMI structures, middle row MBP staining and the bottom row gives the SMI staining pattern. Arrows indicate examples of unmyelinated nerve fibers. Scale bars, 1.15 µm. Right: Enlarged detail of superposed immunostainings and corresponding isosurface-based fitted particles. Images were taken from a control mouse. (e) Statistical analysis of MBP data obtained with expansion microscopy. Depicted are notched box plots of the density (summed intensity divided by volume, left) of the MBP isosurface particles. Data were collected from 4 slices (from 2 control mice, gray, and 2 Kir4.1 ko mice, orange). In each slice, 4 ROIs were analyzed (position of ROIs is shown to the right). A total of 5107 and 3828 particles were analyzed for control and Kir4.1 ko mice, respectively. In each individual ROI of slices from Kir4.1 ko mice, the density was significantly higher than in the corresponding controls (Kruskal–Wallis test) (ROI1, increase to 201%, p < .001; ROI2, to 188%, p < .001; ROI3, to 141%, $p = 0.028$; and ROI4 to 237%, p < .001). Data are given as median ± SEM. Box 25–75 percentile, whiskers ±1.5 IQR, notches ±1.58 IQR/ $\sqrt{n}$, dots show outliers. sr, st. radiatum; slm, st. lacunosum-moleculare; sp, st. pyramidale.

hippocampal age-dependent changes, both in humans (Kaplan et al., 2014; Muffato et al., 2019) and in mice (Kwapis et al., 2020). We noted that enhanced novelty recognition could also lead to a better performance in the NOLR test. General novelty recognition and NOLR are both dependent on activity in the hippocampal CA1. On the other hand, generally increased novelty detection would lead

to an enhanced partner recognition ability, which was not the case in our mice. Thus, we conclude that changes occurring in the hippocampus upon deletion of Kir4.1 in NG2 glia affect memory performance differently, with some behavioral tasks being more susceptible to the deletion-induced alterations than others. Nevertheless, general hippocampal memory deficits and motor deficits were not observed. Since the behavioral tests indicated dysfunction of the hippocampus, the following analyses were focused on that brain region, to unravel underlying mechanisms on the cellular and molecular levels.

4.2 | Targeted deletion of Kir4.1 channels amplifies synaptic input onto NG2 glia

In contrast to astrocytes and oligodendrocytes, hippocampal NG2 glia are not coupled by gap junctions (Griemsmann et al., 2015; Wallraff et al., 2004) and spatial buffering of K^+, which utilizes Kir4.1 channels in the other glial cell types (Larson et al., 2018; Schirmer et al., 2018; Wallraff et al., 2006) is unlikely to occur. Nevertheless, a significant developmental upregulation of inward rectifying currents has been observed in NG2 glia (Kressin et al., 1995;Maldonado et al., 2013), which is mostly mediated by Kir4.1 channels (Djukic et al., 2007;Tang et al., 2009; Song et al., 2018). K^+ fluctuations induced by neuronal activity may be sensed by adult gray matter NG2 glia, and trains of neuronal stimulation may depolarize adult NG2 glia and modulate synaptic currents (Maldonado et al., 2013). Variable Kir current amplitudes were not only observed during development but also between brain regions, with white matter NG2 glia displaying lower current densities than cells in gray matter (Chittajallu et al., 2004). In our study, genetic deletion of Kir4.1 channels led to a tenfold increase in input resistance, similar to what was observed when Ba^{2+} was used to block Kir channels (Chan et al., 2013). The latter study has shown that increase in R_M in thin processes broadens the time window of temporal summation of synaptic signals in NG2 glia, as also predicted in a cable model. Indeed, we observed much larger and longer spontaneous and evoked PSPs in Kir4.1 deficient cells indicating enhanced summation of synaptic input onto NG2 glia, which might activate voltage-activated Ca^{2+} channels (Haberlandt et al., 2011;Sun et al., 2016). The mPSC amplitudes remained unchanged, indicating that K^+ channel deletion did not affect presynaptic release machinery or the structure of postsynaptic glial receptors. However, activation and inactivation kinetics of mPSCs and ePSCs were slower in the knockout cells, which might have been due to altered glutamate clearance in the synaptic cleft. We have previously observed slower PSC kinetics in NG2 glia with high (juvenile stage) vs. lower input resistance (adult) (Passlick et al., 2016). Whether these changes were caused by changes in synaptic structure and surrounding neuropil as observed in developing cerebellar (Cathala et al., 2005) remains to be elucidated. Our study confirms that Kir4.1 channels mediate the main K^+ conductance in adult NG2 glia. We demonstrate that these channels not only determine passive membrane properties but also regulate the efficiency of their depolarization upon synaptic input.

In the naive hippocampus, a single NG2 glial cell receives input from less than 20 glutamatergic neurons, and the GABAergic input is even weaker (Bergles et al., 2000; Haberlandt et al., 2011; Sun & Dietrich, 2013). Notably, short-term synaptic plasticity, which is a measure of vesicle release probability and related to presynaptic Ca^{2+} levels (Zucker & Regehr, 2002), was not affected in Kir4.1 deficient NG2 glia synapses.

4.3 | Deletion of Kir4.1 in NG2 glia only marginally affects proliferation and differentiation but increases MBP density

Global knockout of Kir4.1 resulted in reduced body development, tremor and premature lethality. In the CNS, the development of oligodendrocytes was impaired and vacuolization of white matter tracts was observed, accompanied by reduced myelination and axonal degeneration (Neusch et al., 2001). Conditional, GFAP promoter-driven Kir4.1 ko mice developed ataxia, seizures, and the number of NG2 glia (at that time still called "complex cells," see Bergles et al., 2010) in the hippocampus was profoundly reduced. NG2 glia remaining in those ko mice lost their negative resting potentials and displayed increased membrane resistance (Djukic et al., 2007). Notably, inducing ablation of Kir4.1 from NG2 glia (this study) or oligodendrocytes (Larson et al., 2018) only at postnatal week 3–4, that is, after onset of myelination, overcame this burdened phenotype.

The amplified synaptic input after Kir4.1 deletion only marginally influenced proliferation of NG2 glia, which agrees with a previous study using a BrdU assay in PDGFRα-CreER-based Kir4.1 ko mice (Larson et al., 2018). Interestingly, reduced numbers of $BrdU^+/Olig2^+$ cells were observed in the spinal cord of newborn mice with constitutive Olig2-Kir4.1 deletion, suggesting that lower proliferation entailed an earlier onset of myelination. The authors also reported reduced numbers of progenitor cells, but enhanced MBP transcript levels in newborn Kir4.1-deficient NG2 glia (Schirmer et al., 2018). Knockdown of Kir4.1 in cultured OPCs did not affect proliferation but impaired myelination and differentiation (Wang et al., 2022). These data should be interpreted with caution because it is known that culture conditions may significantly affect glial cell properties. Our NG2-induced deletion of Kir4.1 at the adult stage increased MBP in the hippocampus not only on the transcript but also on the protein level. Tamoxifen-induced recombination in NG2-CreERT2 mice allowed us to track cell fate. We found some cells, both in the hippocampus of control and Kir4.1 ko mice, co-expressing GSTpi with EYFP 8 weeks after tamoxifen injection, indicating differentiation of NG2 glia into oligodendrocytes (Tamura et al., 2007; Huang et al., 2014). Differentiation was particularly evident in the st. lacunosum-moleculare. Variable expression of growth factors, such as PDGF, FGF-2, NT-3 and NGF, or its receptors, might account for subregional differences in proliferation and differentiation (Wilson et al., 2003; Barres et al., 1994;Cohen et al., 1996; Mason & Goldman, 2002).

Since there were only minor differences in the proliferation rate of NG2 glia, and no differences in the density of $GSTpi^+$ cells between

genotypes we conclude that targeted deletion of Kir4.1 did not significantly stimulate NG2 glia differentiation in the hippocampus. This is in line with a study by Larson et al. (2018) who found no changes in NG2 glia differentiation 2 weeks after tamoxifen-induced Kir4.1 from PDGFRα-expressing cells. Thus, the enhanced MBP expression we observed in the hippocampus of Kir4.1 ko mice was unlikely to be due to onset of myelination of former NG2 glia. Rather, lack of Kir4.1 in NG2 glia might have stimulated myelination in already existing oligodendrocytes. Indeed, adaptive myelination and MBP expression depend on neuronal activity and neuron–glia interactions (Bechler et al., 2018; Timmler & Simons, 2019) and NG2 glia contacting nodes of Ranvier may sense the status of myelination (Serwanski et al., 2017).

Gray matter myelination continues throughout adulthood and includes both, formation of new and plasticity of already established myelin internodes (Hill et al., 2018; Hughes et al., 2018). To further evaluate how deletion of Kir4.1 from NG2 glia affected myelination, expansion microscopy was performed allowing for higher (factors 4–5) spatial resolution than conventional confocal microscopy (Chen et al., 2015; Chozinski et al., 2016). MBP is only one among several myelin components, however its strong impact on myelin compactness (DeBruin et al., 2005) makes it an useful measure to assess myelination. We found increased density of MBP in the myelin sheaths as a consequence of targeted deletion of Kir 4.1. Possibly, enhanced Ca^{2+} signaling in oligodendrocytes lacking Kir4.1 underlies enhanced MBP expression and myelin formation (Zhang et al., 2019).

The improved performance in the NOLR test of our NG2 Kir 4.1 ko mice thus might have resulted from increased myelin compactness. Indeed, several previous studies have reported that myelination deficits are accompanied by impaired cognitive performance (Geraghty et al., 2019), social isolation (Makinodan et al., 2012) or deficits in spatial memory and motor skills (McKenzie et al., 2014; Xiao et al., 2016; Steadman et al., 2020). Myelin ensheathment and MBP compactness coordinate temporal regulation and synchronicity of neuronal firing and circuit function (Salami et al., 2003; Seidl, 2014) as well as speed of action potential propagation (Min et al., 2009), and its impairment results in dispersed synaptic transmission, asynchronous firing and deficits in motor learning.

4.4 | Kir4.1 ko mice display impaired hippocampal LTP which is rescued by TrkB receptor activation

Deletion of Kir4.1 from NG2 glia not only affected neuron-NG2 glia communication but also altered neuronal network function and animal behavior. Basal excitability of CA1 neurons and vesicle release probability were not altered, but field potential recordings at the CA3 - CA1 synapse revealed impaired LTP in mice lacking Kir4.1 in NG2 glia indicating functional alterations at the postsynaptic site. Conditional deletion of Kir4.1 from all macroglia resulted in enhanced LTP at the same synapse (Djukic et al., 2007), presumably due to impaired K^+ and glutamate homeostasis, that is, functions through which astrocytes regulate neuronal excitability (Katagiri et al., 2001; Wallraff et al., 2006; Filosa et al., 2009; Chever et al., 2010; Sibille et al., 2014). In the somatosensory cortex, shedding of the NG2 ectodomain is required for proper LTP, probably by facilitating expression of Ca^{2+} impermeable AMPA receptors (Sakry et al., 2014), although deletion of NG2 did not affect LTP in the hippocampus (Passlick et al., 2016). There is compelling evidence for a critical role of BDNF–TrkB signaling in the induction and maintenance of hippocampal LTP (Korte et al., 1995; Minichiello et al., 1999; Chen et al., 1999). We tested whether in our NG2 glia-specific Kir4.1 ko mice, activation of TrkB receptors would restore LTP. Indeed, extracellular application of the TrkB receptor agonist 7,8-DHF completely rescued LTP, indicating that extracellular BDNF levels rather than TrkB receptor expression was disturbed in the knockout mice. Notably, the impairment of plasticity seemed to concern a majority of hippocampal synapses, despite the limited efficiency of Kir4.1 deletion in NG2 glia. Besides neurons, microglia and astrocytes contribute to BDNF release, which induces neuronal activation and synaptic plasticity (Fernandez-Garcia et al., 2020; Parkhurst et al., 2013). It is thus conceivable that microglia or astrocytes, which individually contact a multitude of synapses (Nimmerjahn et al., 2005; Ventura & Harris, 1999), have been affected by dysfunctional NG2 glia. However, cultured NG2 glia-like cells may also release BDNF (Prasad et al., 2017; Tanaka et al., 2009). Thus, an additional obvious possibility would be that NG2 glia after Kir4.1 deletion release reduced BDNF, which impairs stimulation of neuronal TrkB receptors and LTP. While BDNF release from neurons is Ca^{2+}-dependent (Blöchl & Thoenen, 1995), the release from cultured NG2 glia was Ca^{2+}-independent (Tanaka et al., 2009). Stimulation of BDNF release by ATP/P2X4 receptors, as shown in microglia (Parkhurst et al., 2013) seems less likely because hippocampal NG2 glia lack this receptor (Jabs et al., 2007). Corresponding investigations are subject of future studies.

Reduced LTP after high-frequency stimulation of Schaffer collaterals in hippocampal slices of Kir4.1 ko mice did not entail deficits in behavioral tests. Instead, mice with targeted deletion of Kir4.1 in NG2 glia showed improved performance in the NOLR test. A negative correlation of CA3-CA1 LTP and behavior, that is, enhanced LTP but impaired behavioral performance, was previously observed after genetic deletion of transcription activator Fmr2 (Gu et al., 2002), PSD-95 (Migaud et al., 1998) or heterozygous deletion of the BDNF receptor TrkB (Minichiello et al., 1999). However, homozygous TrkB receptor knockout caused decreased LTP and behavioral impairment suggesting that only profound LTP reduction affects behavior (Minichiello et al., 1999; Qi et al., 1996).

5 | CONCLUSIONS

Activity-dependent myelination is an important mechanism to ensure proper synaptic function and spiking synchronicity, motor skills and memory performance. Our data imply that these processes are also influenced by NG2 glia and that this is not simply dependent on their differentiation status. Rather, it is likely that NG2 glia exert its effect by signaling on neighboring oligodendrocytes, either directly or

indirectly via influencing neuronal activity. Future work has to identify the mechanisms and factors by which NG2 glia accomplish these actions. Although causal relationships remain to be established, the current study shows that Kir4.1 expression by NG2 glia is important for many aspects of hippocampal function and also for a type of memory that typically relies on the hippocampus.

AUTHOR CONTRIBUTIONS

CS, GS: study concept; AT, DT, AB, CD, MS, GS, RJ, AB-K, CS: aquisition and evaluation of data; CS, GS, WH, FK, CH, AB-K: provision of resources and funding; AT, AB, CD, AB-K, RJ, GS, CS: drafting of the manuscript; DT, RJ, WH, FK, CH, GS, CS: finalization of the manuscript.

ACKNOWLEDGMENTS

We thank T. Erdmann for technical assistance.

This work was supported by Deutsche Forschungsgemeinschaft (SPP1757: STE 552/5 to CS, SE 774/6 to GS, HE6949/1 to CH, and HE6949/3 to CH). Open Access funding enabled and organized by Projekt DEAL.

CONFLICT OF INTEREST STATEMENT

The authors declare no competing interests.

DATA AVAILABILITY STATEMENT

All data generated or analysed during this study are included in the manuscript and supplemental files; any additional Source Data files areprovided by the authors on request.

ORCID

Wenhui Huang https://orcid.org/0000-0001-9865-0375
Frank Kirchhoff https://orcid.org/0000-0002-2324-2761
Christian Henneberger https://orcid.org/0000-0002-5391-7387
Andras Bilkei-Gorzo https://orcid.org/0000-0002-6805-0472
Christian Steinhäuser https://orcid.org/0000-0003-2579-8357

REFERENCES

Albayram, O., Passlick, S., Bilkei-Gorzo, A., Zimmer, A., & Steinhäuser, C. (2016). Physiological impact of CB1 receptor expression by hippocampal GABAergic interneurons. *Pflügers Archiv*, *468*, 727–737.

Albrecht, S., Korr, S., Nowack, L., Narayanan, V., Starost, L., Stortz, F., Rauzo-Bravo, M. J., Meuth, S. G., Kuhlmann, T., & Hundehege, P. (2019). The K2P -channel TASK1 affects Oligodendroglial differentiation but not myelin restoration. *Glia*, *67*, 870–883.

Asano, S. M., Gao, R., Wassie, A. T., Tillberg, P. W., Chen, F., & Boyden, E. S. (2018). Expansion microscopy: Protocols for imaging proteins and RNA in cells and tissues. *Current Protocols in Cell Biology*, *80*, e56.

Barres, B. A., Raff, M. C., Gaese, F., Bartke, I., Dechant, G., & Barde, Y.-A. (1994). A crucial role for neurotrophin-3 in oligodendrocyte development. *Nature*, *367*, 371–375.

Bechler, M. E., Swire, M., & Ffrench-Constant, C. (2018). Intrinsic and adaptive myelination-A sequential mechanism for smart wiring in the brain. *Developmental Neurobiology*, *78*, 68–79.

Bergles, D. E., Jabs, R., & Steinhäuser, C. (2010). Neuron-glia synapses in the brain. *Brain Research Reviews*, *63*, 130–137.

Bergles, D. E., Roberts, J. D., Somogyi, P., & Jahr, C. E. (2000). Glutamatergic synapses on oligodendrocyte precursor cells in the hippocampus. *Nature*, *405*, 187–191.

Bilkei-Gorzo, A., Albayram, O., Draffehn, A., Michel, K., Piyanova, A., Oppenheimer, H., Dvir-Ginzberg, M., Racz, I., Ulas, T., Imbeault, S., Bab, I., Schultze, J. L., & Zimmer, A. (2017). A chronic low dose of Delta(9)-tetrahydrocannabinol (THC) restores cognitive function in old mice. *Nature Medicine*, *23*, 782–787.

Birey, F., Kloc, M., Chavali, M., Hussein, I., Wilson, M., Christoffel, D. J., Chen, T., Frohman, M. A., Robinson, J. K., Russo, S. J., Maffei, A., & Aguirre, A. (2015). Genetic and stress-induced loss of NG2 glia triggers emergence of depressive-like behaviors through reduced secretion of FGF2. *Neuron*, *88*, 941–956.

Blöchl, A., & Thoenen, H. (1995). Characterization of nerve growth factor (NGF) release from hippocampal neurons: Evidence for a constitiutive and an unconventional sodium-dependent regulated pathway. *The European Journal of Neuroscience*, *7*, 1220–1228.

Cathala, L., Holderith, N. B., Nusser, Z., DiGregorio, D. A., & Cull-Candy, S. G. (2005). Changes in synaptic structure underlie the developmental speeding of AMPA receptor-mediated EPSCs. *Nature Neuroscience*, *8*, 1310–1318.

Chan, C. F., Kuo, T. W., Weng, J. Y., Lin, Y. C., Chen, T. Y., Cheng, J. K., & Lien, C. C. (2013). Ba2+− and bupivacaine-sensitive background K+ conductances mediate rapid EPSP attenuation in oligodendrocyte precursor cells. *The Journal of Physiology*, *591*, 4843–4858.

Chen, F., Tillberg, P. W., & Boyden, E. S. (2015). Optical imaging. Expansion microscopy. *Science*, *347*, 543–548.

Chen, G., Kolbeck, R., Barde, Y. A., Bonhoeffer, T., & Kossel, A. (1999). Relative contribution of endogenous neurotrophins in hippocampal long-term potentiation. *The Journal of Neuroscience*, *19*, 7983–7990.

Chen, J. F., Huang, Z., Ma, J., Zhu, J., Moratalla, R., Standaert, D., Moskowitz, M. A., Fink, J. S., & Schwarzschild, M. A. (1999). A (2A) adenosine receptor deficiency attenuates brain injury induced by transient focal ischemia in mice. *The Journal of Neuroscience*, *19*, 9192–9200.

Chever, O., Djukic, B., McCarthy, K. D., & Amzica, F. (2010). Implication of kir4.1 channel in excess potassium clearance: An in vivo study on anesthetized glial-conditional kir4.1 knock-out mice. *The Journal of Neuroscience*, *30*, 15769–15777.

Chittajallu, R., Aguirre, A., & Gallo, V. (2004). NG2-positive cells in the mouse white and grey matter display distinct physiological properties. *The Journal of Physiology*, *561*, 109–122.

Chozinski, T. J., Halpern, A. R., Okawa, H., Kim, H. J., Tremel, G. J., Wong, R. O., & Vaughan, J. C. (2016). Expansion microscopy with conventional antibodies and fluorescent proteins. *Nature Methods*, *13*, 485–488.

Cohen, R. I., Marmur, R., Norton, W. T., Mehler, M. F., & Kessler, J. A. (1996). Nerve growth factor and neurotrophin-3 differentially regulate the proliferation and survival of developing rat brain oligodendrocytes. *The Journal of Neuroscience*, *16*, 6433–6442.

DeBruin, L. S., Haines, J. D., Wellhauser, L. A., Radeva, G., Schonmann, V., Bienzle, D., & Harauz, G. (2005). Developmental partitioning of myelin basic protein into membrane microdomains. *Journal of Neuroscience Research*, *80*, 211–225.

Degen, J., Dublin, P., Zhang, J., Dobrowolski, R., Jokwitz, M., Karram, K., Trotter, J., Jabs, R., Willecke, K., Steinhäuser, C., & Theis, M. (2012). Dual reporter approaches for identification of Cre efficacy and astrocyte heterogeneity. *The FASEB Journal*, *26*, 4576–4583.

Deshpande, T., Li, T., Herde, M. K., Becker, A., Vatter, H., Schwarz, M. K., Henneberger, C., Steinhuser, C., & Bedner, P. (2017). Subcellular reorganization and altered phosphorylation of the astrocytic gap junction protein connexin43 in human and experimental temporal lobe epilepsy. *Glia*, *65*, 1809–1820.

Diers-Fenger, M., Kirchhoff, F., Kettenmann, H., Levine, J. M., & Trotter, J. (2001). AN2/NG2 protein-expressing glial progenitor cells in the murine CNS: Isolation, differentiation, and association with radial glia. *Glia*, *34*, 213–228.

Dimou, L., Simon, C., Kirchhoff, F., Takebayashi, H., & Gotz, M. (2008). Progeny of Olig2-expressing progenitors in the gray and white matter of the adult mouse cerebral cortex. *The Journal of Neuroscience*, *28*, 10434–10442.

Djukic, B., Casper, K. B., Philpot, B. D., Chin, L. S., & McCarthy, K. D. (2007). Conditional knock-out of Kir4.1 leads to glial membrane depolarization, inhibition of potassium and glutamate uptake, and enhanced short-term synaptic potentiation. *The Journal of Neuroscience*, *27*, 11354–11365.

Fernandez-Garcia, S., Sancho-Balsells, A., Longueville, S., Herve, D., Gruart, A., gado-Garcia, J.M., Alberch, J., & Giralt, A. (2020). Astrocytic BDNF and TrkB regulate severity and neuronal activity in mouse models of temporal lobe epilepsy. *Cell Death & Disease*, *11*, 411.

Filosa, A., Paixao, S., Honsek, S. D., Carmona, M. A., Becker, L., Feddersen, B., Gaitanos, L., Rudhard, Y., Schoepfer, R., Klopstock, T., Kullander, K., Rose, C. R., Pasquale, E. B., & Klein, R. (2009). Neuron-glia communication via EphA4/ephrin-A3 modulates LTP through glial glutamate transport. *Nature Neuroscience*, *12*, 1285–1292.

Geraghty, A. C., Gibson, E. M., Ghanem, R. A., Greene, J. J., Ocampo, A., Goldstein, A. K., Ni, L., Yang, T., Marton, R. M., Pasca, S. P., Greenberg, M. E., Longo, F. M., & Monje, M. (2019). Loss of adaptive myelination contributes to methotrexate chemotherapy-related cognitive impairment. *Neuron*, *103*, 250–265.

Griemsmann, S., Hft, S. P., Bedner, P., Zhang, J., von Staden, E., Beinhauer, A., Degen, J., Dublin, P., Cope, D. W., Richter, N., Crunelli, V., Jabs, R., Willecke, K., Theis, M., Seifert, G., Kettenmann, H., & Steinhäuser, C. (2015). Characterization of Panglial gap junction networks in the thalamus, neocortex, and hippocampus reveals a unique population of glial cells. *Cerebral Cortex*, *25*, 3420–3433.

Gu, Y., McIlwain, K. L., Weeber, E. J., Yamagata, T., Xu, B., Antalffy, B. A., Reyes, C., Yuva-Paylor, L., Armstrong, D., Zoghbi, H., Sweatt, J. D., Paylor, R., & Nelson, D. L. (2002). Impaired conditioned fear and enhanced long-term potentiation in Fmr2 knock-out mice. *The Journal of Neuroscience*, *22*, 2753–2763.

Haberlandt, C., Derouiche, A., Wyczynski, A., Haseleu, J., Pohle, J., Karram, K., Trotter, J., Seifert, G., Frotscher, M., Steinhäuser, C., & Jabs, R. (2011). Gray matter NG2 cells display multiple Ca-signaling pathways and highly motile processes. *PLoS One*, *6*, e17575.

Herde, M. K., Bohmbach, K., Domingos, C., Vana, N., Komorowska-Muller, J. A., Passlick, S., Schwarz, I., Jackson, C. J., Dietrich, D., Schwarz, M. K., & Henneberger, C. (2020). Local efficacy of glutamate uptake decreases with synapse size. *Cell Reports*, *32*, 108182.

Hill, R. A., Li, A. M., & Grutzendler, J. (2018). Lifelong cortical myelin plasticity and age-related degeneration in the live mammalian brain. *Nature Neuroscience*, *21*, 683–695.

Huang, W., Zhao, N., Bai, X., Karram, K., Trotter, J., Goebbels, S., Scheller, A., & Kirchhoff, F. (2014). Novel NG2-CreERT2 knock-in mice demonstrate heterogeneous differentiation potential of NG2 glia during development. *Glia*, *62*, 896–913.

Hughes, E. G., Orthmann-Murphy, J. L., Langseth, A. J., & Bergles, D. E. (2018). Myelin remodeling through experience-dependent oligodendrogenesis in the adult somatosensory cortex. *Nature Neuroscience*, *21*, 696–706.

Jabs, R., Matthias, K., Grote, A., Grauer, M., Seifert, G., & Steinhäuser, C. (2007). Lack of P2X receptor mediated currents in astrocytes and GluR type glial cells of the hippocampal CA1 region. *Glia*, *55*, 1648–1655.

Jabs, R., Pivneva, T., Hüttmann, K., Wyczynski, A., Nolte, C., Kettenmann, H., & Steinhäuser, C. (2005). Synaptic transmission onto hippocampal glial cells with hGFAP promoter activity. *Journal of Cell Science*, *118*, 3791–3803.

Jang, S. W., Liu, X., Yepes, M., Shepherd, K. R., Miller, G. W., Liu, Y., Wilson, W. D., Xiao, G., Blanchi, B., Sun, Y. E., & Ye, K. (2010). A selective TrkB agonist with potent neurotrophic activities by 7,8-dihydroxyflavone. *Proceedings of the National Academy of Sciences of the United States of America*, *107*, 2687–2692.

Kang, S. H., Fukaya, M., Yang, J. K., Rothstein, J. D., & Bergles, D. E. (2010). NG2+ CNS glial progenitors remain committed to the oligodendrocyte lineage in postnatal life and following neurodegeneration. *Neuron*, *68*, 668–681.

Kaplan, R., Horner, A. J., Bandettini, P. A., Doeller, C. F., & Burgess, N. (2014). Human hippocampal processing of environmental novelty during spatial navigation hippocampus. *Hippocampus*, *24*, 740–750.

Karram, K., Goebbels, S., Schwab, M., Jennissen, K., Seifert, G., Steinhäuser, C., Nave, K. A., & Trotter, J. (2008). NG2-expressing cells in the nervous system revealed by the NG2-EYFP-knockin mouse. *Genesis*, *46*, 743–757.

Katagiri, H., Tanaka, K., & Manabe, T. (2001). Requirement of appropriate glutamate concentrations in the synaptic cleft for hippocampal LTP induction. *The European Journal of Neuroscience*, *14*, 547–553.

Korte, M., Carroll, P., Wolf, E., Brem, G., Thoenen, H., & Bonhoeffer, T. (1995). Hippocampal long-term potentiation is impaired in mice lacking brain-derived neurotrophic factor. *Proceedings of the National Academy of Sciences of the United States of America*, *92*, 8856–8860.

Kougioumtzidou, E., Shimizu, T., Hamilton, N. B., Tohyama, K., Sprengel, R., Monyer, H., Attwell, D., & Richardson, W. D. (2017). Signalling through AMPA receptors on oligodendrocyte precursors promotes myelination by enhancing oligodendrocyte survival. *eLife*, *6*, e28080.

Kressin, K., Kuprijanova, E., Jabs, R., Seifert, G., & Steinhäuser, C. (1995). Developmental regulation of Na^+ and K^+ conductances in glial cells of mouse hippocampal brain slices. *Glia*, *15*, 173–187.

Kwapis, J. L., Alaghband, Y., Keiser, A. A., Dong, T. N., Michael, C. M., Rhee, D., Shu, G., Dang, R. T., Matheos, D. P., & Wood, M. A. (2020). Aging mice show impaired memory updating in the novel OUL updating paradigm. *Neuropsychopharmacology*, *45*, 337–346.

Lalonde, R. (2002). The neurobiological basis of spontaneous alternation. *Neuroscience and Biobehavioral Reviews*, *26*, 91–104.

Larkin, M. C., Lykken, C., Tye, L. D., Wickelgren, J. G., & Frank, L. M. (2014). Hippocampal output area CA1 broadcasts a generalized novelty signal during an object-place recognition task. *Hippocampus*, *24*, 773–783.

Larson, V. A., Mironova, Y., Vanderpool, K. G., Waisman, A., Rash, J. E., Agarwal, A., & Bergles, D. E. (2018). Oligodendrocytes control potassium accumulation in white matter and seizure susceptibility. *eLife*, *7*, e34829.

Lin, S. C., & Bergles, D. E. (2004). Synaptic signaling between GABAergic interneurons and oligodendrocyte precursor cells in the hippocampus. *Nature Neuroscience*, *7*, 24–32.

Liu, Y., & Aguzzi, A. (2020). NG2 glia are required for maintaining microglia homeostatic state. *Glia*, *68*, 345–355.

Lynch, M. A. (2004). Long-term potentiation and memory. *Physiological Reviews*, *84*, 87–136.

Makinodan, M., Rosen, K. M., Ito, S., & Corfas, G. (2012). A critical period for social experience-dependent oligodendrocyte maturation and myelination. *Science*, *337*, 1357–1360.

Maldonado, P. P., Velez-Fort, M., Levavasseur, F., & Angulo, M. C. (2013). Oligodendrocyte precursor cells are accurate sensors of local K+ in mature gray matter. *The Journal of Neuroscience*, *33*, 2432–2442.

Marisca, R., Hoche, T., Agirre, E., Hoodless, L. J., Barkey, W., Auer, F., Castelo-Branco, G., & Czopka, T. (2020). Functionally distinct subgroups of oligodendrocyte precursor cells integrate neural activity and execute myelin formation. *Nature Neuroscience*, *23*, 363–374.

Mason, J. L., & Goldman, J. E. (2002). A2B^{5+} and O^{4+} cycling progenitors in the adult forebrain white matter respond differentially to PDGF-AA, FGF-2, and IGF-1. *Molecular and Cellular Neurosciences*, *20*, 30–42.

Matthias, K., Kirchhoff, F., Seifert, G., Hüttmann, K., Matyash, M., Kettenmann, H., & Steinhäuser, C. (2003). Segregated expression of AMPA-type glutamate receptors and glutamate transporters defines distinct astrocyte populations in the mouse hippocampus. *The Journal of Neuroscience*, *23*, 1750–1758.

McKenzie, I. A., Ohayon, D., Li, H., de Faria, J. P., Emery, B., Tohyama, K., & Richardson, W. D. (2014). Motor skill learning requires active central myelination. *Science*, *346*, 318–322.

Migaud, M., Charlesworth, P., Dempster, M., Webster, L. C., Watabe, A. M., Makhinson, M., He, Y., Ramsay, M. F., Morris, R. G. M., Morrison, J. H., & O'Dell, T. J. (1998). Enhanced long-term potentiation and impaired learning in mice with mutant postsynaptic density-95 protein. *Nature*, *396*, 433–439.

Min, Y., Kristiansen, K., Boggs, J. M., Husted, C., Zasadzinski, J. A., & Israelachvili, J. (2009). Interaction forces and adhesion of supported myelin lipid bilayers modulated by myelin basic protein. *Proceedings of the National Academy of Sciences of the United States of America*, *106*, 3154–3159.

Minichiello, L., Korte, M., Wolfer, D., Kühn, R., Unsicker, K., Cestari, V., Rossi-Arnaud, C., Lipp, H. P., Bonhoeffer, T., & Klein, R. (1999). Essential role for TrkB receptors in hippocampus-mediated learning. *Neuron*, *24*, 401–414.

Mongiat, L. A., Esposito, M. S., Lombardi, G., & Schinder, A. F. (2009). Reliable activation of immature neurons in the adult hippocampus. *PLoS One*, *4*, e5320.

Moshrefi-Ravasdjani, B., Dublin, P., Seifert, G., Jennissen, K., Steinhuser, C., Kafitz, K. W., & Rose, C. R. (2017). Changes in the proliferative capacity of NG2 cell subpopulations during postnatal development of the mouse hippocampus. *Brain Structure & Function*, *222*, 831–847.

Muffato, V., Hilton, C., Meneghetti, C., De Beni, R., & Wiener, J. M. (2019). Evidence for age-related deficits in object-location binding during place recognition. *Hippocampus*, *29*, 971–979.

Neusch, C., Rozengurt, N., Jacobs, R. E., Lester, H. A., & Kofuji, P. (2001). Kir4.1 potassium channel subunit is crucial for oligodendrocyte development and in vivo myelination. *The Journal of Neuroscience*, *21*, 5429–5438.

Nimmerjahn, A., Kirchhoff, F., & Helmchen, F. (2005). Resting microglial cells are highly dynamic surveillants of brain parenchyma in vivo. *Science*, *308*, 1314–1318.

Nishiyama, A., Komitova, M., Suzuki, R., & Zhu, X. (2009). Polydendrocytes (NG2 cells): Multifunctional cells with lineage plasticity. *Nature Reviews. Neuroscience*, *10*, 9–22.

Parkhurst, C. N., Yang, G., Ninan, I., Savas, J. N., Yates, J. R., III, Lafaille, J. J., Hempstead, B. L., Littman, D. R., & Gan, W. B. (2013). Microglia promote learning-dependent synapse formation through brain-derived neurotrophic factor. *Cell*, *155*, 1596–1609.

Passlick, S., Grauer, M., Schafer, C., Jabs, R., Seifert, G., & Steinhäuser, C. (2013). Expression of the gamma2-subunit distinguishes synaptic and extrasynaptic GABA(A) receptors in NG2 cells of the hippocampus. *The Journal of Neuroscience*, *33*, 12030–12040.

Passlick, S., Trotter, J., Seifert, G., Steinhäuser, C., & Jabs, R. (2016). The NG2 protein is not required for glutamatergic neuron-NG2 cell synaptic signaling. *Cerebral Cortex*, *26*, 51–57.

Peters, A. (2004). A fourth type of neuroglial cell in the adult central nervous system. *Journal of Neurocytology*, *33*, 345–357.

Phillmore, L. S., & Klein, R. M. (2019). The puzzle of spontaneous alternation and inhibition of return: How they might fit together. *Hippocampus*, *29*, 762–770.

Prasad, A., Teh, D. B. L., Blasiak, A., Chai, C., Wu, Y., Gharibani, P. M., Yang, I. H., Phan, T. T., Lim, K. L., Yang, H., Liu, X., & All, A. H. (2017). Static magnetic field stimulation enhances oligodendrocyte differentiation and secretion of neurotrophyic factors. *Scientific Reports*, *7*, 6743.

Qi, M., Zhuo, M., Skalhegg, B. S., Brandon, E. P., Kandel, E. R., McKnight, G. S., & Idzerda, R. L. (1996). Impaired hippocampal plasticity in mice lacking the Cbeta1 catalytic subunit of cAMP-dependent protein kinase. *Proceedings of the National Academy of Sciences of the United States of America*, *93*, 1571–1576.

R Core Team. (2020). *2020. R: A language and environment for statistical computing. R Foundation for Statistical Computing*. Vienna http://www.r-project org/index html

Rivers, L. E., Young, K. M., Rizzi, M., Jamen, F., Psachoulia, K., Wade, A., Kessaris, N., & Richardson, W. D. (2008). PDGFRA/NG2 glia generate myelinating oligodendrocytes and piriform projection neurons in adult mice. *Nature Neuroscience*, *11*, 1392–1401.

Sakry, D., Neitz, A., Singh, J., Frischknecht, R., Marongiu, D., Biname, F., Perera, S. S., Endres, K., Lutz, B., Radyushkin, K., Trotter, J., & Mittmann, T. (2014). Oligodendrocyte precursor cells modulate the neuronal network by activity-dependent ectodomain cleavage of glial NG2. *PLoS Biology*, *12*, e1001993.

Salami, M., Itami, C., Tsumoto, T., & Kimura, F. (2003). Change of conduction velocity by regional myelination yields constant latency irrespective of distance between thalamus and cortex. *Proceedings of the National Academy of Sciences of the United States of America*, *100*, 6174–6179.

Schirmer L, Mobius W, Zhao C, Cruz-Herranz A, Ben HL, Cordano C, Shiow LR, Kelley KW, Sadowski B, Timmons G, Probstel AK, Wright JN, Sin JH, Devereux M, Morrison DE, Chang SM, Sabeur K, Green AJ, Nave KA, Franklin RJ, Rowitch DH. 2018. Oligodendrocyte-encoded Kir4.1 function is required for axonal integrity. Elife 7.

Schröder, W., Seifert, G., Hüttmann, K., Hinterkeuser, S., & Steinhäuser, C. (2002). AMPA receptor-mediated modulation of inward rectifier k(+) channels in astrocytes of mouse hippocampus. *Molecular and Cellular Neurosciences*, *19*, 447–458.

Seidl, A. H. (2014). Regulation of conduction time along axons. *Neuroscience*, *276*, 126–134.

Seifert, G., & Steinhäuser, C. (2018). Heterogeneity and function of hippocampal macroglia. *Cell and Tissue Research*, *373*, 653–670.

Serwanski, D. R., Jukkola, P., & Nishiyama, A. (2017). Heterogeneity of astrocyte and NG2 cell insertion at the node of ranvier. *The Journal of Comparative Neurology*, *525*, 535–552.

Sibille, J., Pannasch, U., & Rouach, N. (2014). Astroglial potassium clearance contributes to short-term plasticity of synaptically evoked currents at the tripartite synapse. *The Journal of Physiology*, *592*, 87–102.

Song, F., Hong, X., Cao, J., Ma, G., Han, Y., Cepeda, C., Kang, Z., Xu, T., Duan, S., Wan, J., & Tong, X. (2018). Kir4.1 channels in NG2-glia play a role in development, potassium signaling, and ischemia-related myelin loss. *Communications Biology*, *1*, 80.

Squire, L. R., & Dede, A. J. (2015). Conscious and unconscious memory systems. *Cold Spring Harbor Perspectives in Biology*, *7*, a021667.

Srinivas, S., Watanabe, T., Lin, C. S., William, C. M., Tanabe, Y., Jessell, T. M., & Costantini, F. (2001). Cre reporter strains produced by targeted insertion of EYFP and ECFP into the ROSA26 locus. *BMC Developmental Biology*, *1*, 4.

Steadman, P. E., Xia, F., Ahmed, M., Mocle, A. J., Penning, A. R. A., Geraghty, A. C., Steenland, H. W., Monje, M., Josselyn, S. A., & Frankland, P. W. (2020). Disruption of Oligodendrogenesis impairs memory consolidation in adult mice. *Neuron*, *105*, 150–164.

Sun, W., & Dietrich, D. (2013). Synaptic integration by NG2 cells. *Frontiers in Cellular Neuroscience*, *7*, 255.

Sun, W., Matthews, E. A., Nicolas, V., Schoch, S., & Dietrich, D. (2016). NG2 glial cells integrate synaptic input in global and dendritic calcium signals. *eLife*, *5*, e16262.

Tamura, Y., Kataoka, Y., Cui, Y., Takamori, Y., Watanabe, Y., & Yamada, H. (2007). Multi-directional differentiation of doublecortin- and NG2-immunopositive progenitor cells in the adult rat neocortex in vivo. *The European Journal of Neuroscience*, *25*, 3489–3498.

Tanaka, Y., Tozuka, Y., Takata, T., Shimazu, N., Matsumara, N., Ohta, A., & Hisatsune, T. (2009). Excitatory GABAergic activation of cortical dividing glial cells. *Cerebral Cortex*, *19*, 2181–2195.

Tang, X., Taniguchi, K., & Kofuji, P. (2009). Heterogeneity of Kir4.1 channel expression in glia revealed by mouse transgenesis. *Glia*, *57*, 1706–1715.

Tansey, F. A., Farooq, M., & Cammer, W. (1991). Glutamine synthetase in oligodendrocytes and astrocytes: New biochemical and immunocytochemical evidence. *Journal of Neurochemistry*, *56*, 266–272.

Timmler, S., & Simons, M. (2019). Grey matter myelination. *Glia*, *67*, 2063–2070.

Trotter, J., Karram, K., & Nishiyama, A. (2010). NG2 cells: Properties, progeny and origin. *Brain Research Reviews*, *63*, 72–82.

Ventura, R., & Harris, K. M. (1999). Three-dimensional relationships between hippocampal synapses and astrocytes. *The Journal of Neuroscience*, *19*, 6897–6906.

Wallraff, A., Kohling, R., Heinemann, U., Theis, M., Willecke, K., & Steinhäuser, C. (2006). The impact of astrocytic gap junctional coupling on potassium buffering in the hippocampus. *The Journal of Neuroscience*, *26*, 5438–5447.

Wallraff, A., Odermatt, B., Willecke, K., & Steinhäuser, C. (2004). Distinct types of astroglial cells in the hippocampus differ in gap junction coupling. *Glia*, *48*, 36–43.

Wang, N., Zhou, L., Shao, C. Y., Wang, X. T., Zhang, N., Ma, J., Hu, H. L., Wang, Y., Qiu, M., & Shen, Y. (2022). Potassium channel Kir4.1 regulates oligodendrocyte differentiation via intracellular pH regulation. *Glia*, *70*, 2093–2107.

Wersinger, S. R., Ginns, E. I., O'Carroll, A. M., Lolait, S. J., & Young, W. S. (2002). Vasopressin V1b receptor knockout reduces aggressive behavior in male mice. *Molecular Psychiatry*, *7*, 975–984.

Wilson, H. C., Onischke, C., & Raine, C. S. (2003). Human oligodendrocyte precursor cells in vitro: Phenotypic analysis and differential response to growth factors. *Glia*, *44*, 153–165.

Xiao, L., Ohayon, D., McKenzie, I. A., Sinclair-Wilson, A., Wright, J. L., Fudge, A. D., Emery, B., Li, H., & Richardson, W. D. (2016). Rapid production of new oligodendrocytes is required in the earliest stages of motor-skill learning. *Nature Neuroscience*, *19*, 1210–1217.

Ye, P., Bagnell, R., & D'Ercole, A. J. (2003). Mouse NG2+ oligodendrocyte precursors express mRNA for proteolipid protein but not its DM-20 variant: A study of laser microdissection-captured NG2+ cells. *The Journal of Neuroscience*, *23*, 4401–4405.

Zhang, J., Miller, M. I., Plachez, C., Richards, L. J., Yarowsky, P., van Zijl, P., & Mori, S. (2005). Mapping postnatal mouse brain development with diffusion tensor microimaging. *NeuroImage*, *26*, 1042–1051.

Zhang, M., Liu, Y., Wu, S., & Zhao, X. (2019). Ca(2+) Signaling in Oligodendrocyte Development. *Cellular and Molecular Neurobiology*, *39*, 1071–1080.

Zucker, R. S., & Regehr, W. G. (2002). Short-term synaptic plasticity. *Annual Review of Physiology*, *64*, 355–405.

SUPPORTING INFORMATION

Additional supporting information can be found online in the Supporting Information section at the end of this article.

How to cite this article: Timmermann, A., Tascio, D., Jabs, R., Boehlen, A., Domingos, C., Skubal, M., Huang, W., Kirchhoff, F., Henneberger, C., Bilkei-Gorzo, A., Seifert, G., & Steinhäuser, C. (2023). Dysfunction of NG2 glial cells affects neuronal plasticity and behavior. *Glia*, *71*(6), 1481–1501. https://doi.org/10.1002/glia.24352